OCTOBER 2025

Volume 1 Issue 4

BIOCONJUGATION INSIGHTS

SPOTLIGHT

Driving improvements in the delivery and stability of next-generation bioconjugates, including oligo, polymer, and enzyme

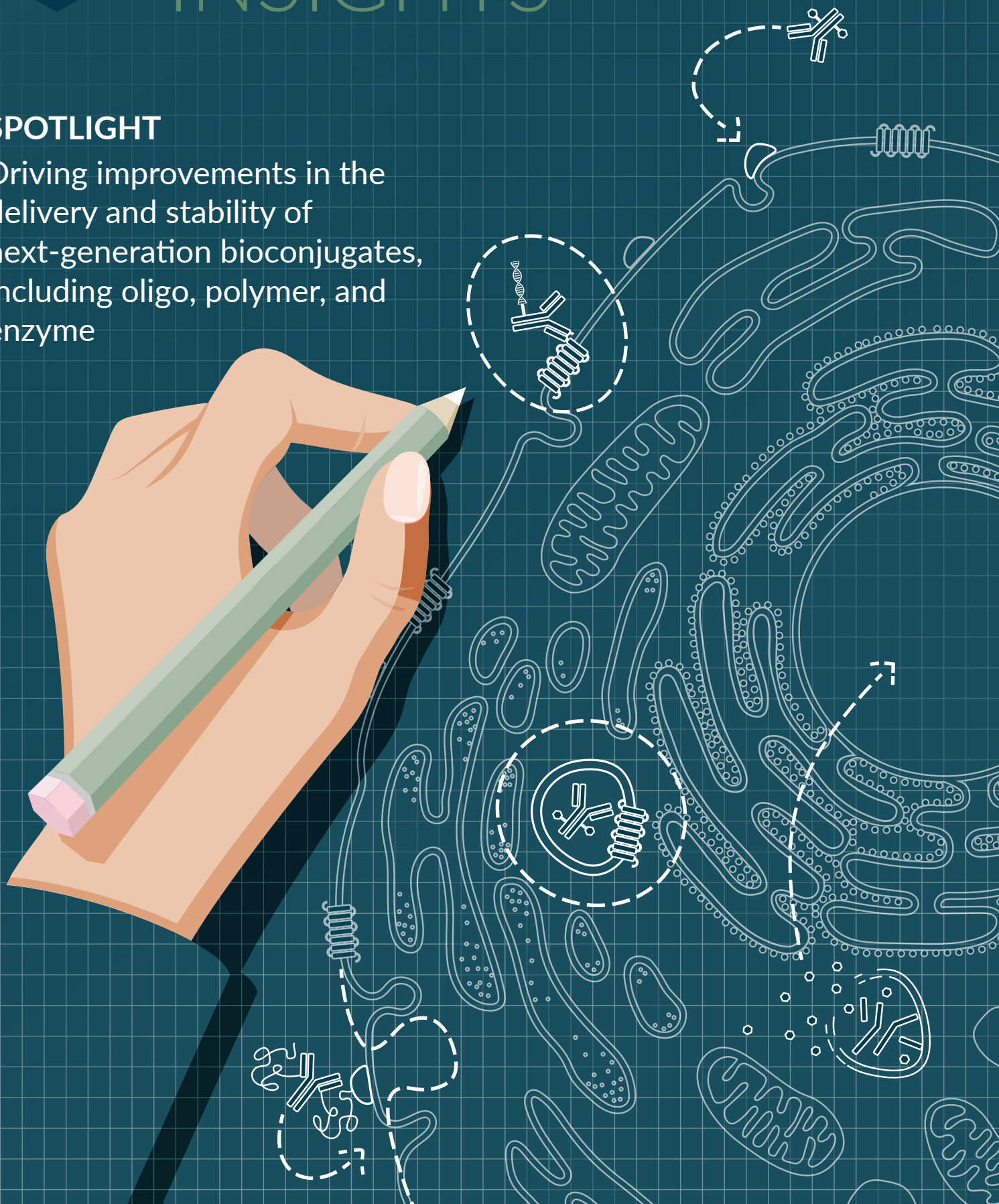

BIOCONJUGATION INSIGHTS

CONTENTS VOLUME 1 · ISSUE 4

Driving improvements in the delivery and stability of next-generation bioconjugates, including oligo, polymer, and enzyme

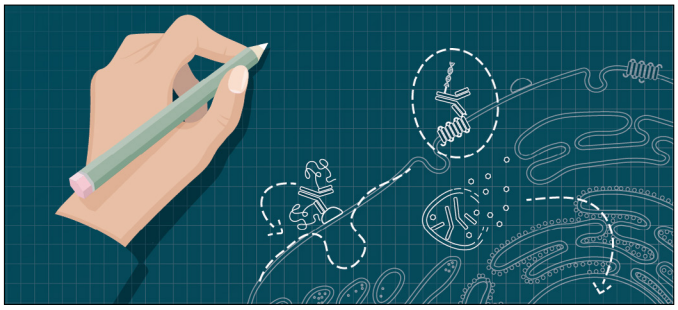

LATEST ARTICLES

BIOCONJUGATION INSIGHTS

DRIVING IMPROVEMENTS IN DELIVERY AND STABILITY

SPOTLIGHT

REVIEW

Strategies for improving endosomal escape of polymeric nanoparticles

Yvonne Yoyo Ma, Parul Sirohi, and Ashutosh Chilkoti

While nanoparticle systems serve as a promising platform for the delivery of small molecule, nucleic acid, and protein-based therapeutics for a variety of diseases, their therapeutic efficacy is currently constrained by poor endosomal escape once internalized. Successful nanoparticle-based delivery entails effective endosomal escape and subsequent cytosolic release of therapeutic cargo, thus it is imperative that nanoparticle platforms integrate endosomal escape moieties into their synthesis. This review will discuss synthetic strategies for nanoparticles that improve endosomal escape, with a focus on strategies compatible with polymer-based nanoparticles. Recent advancements in polymer, small molecule, and peptide-based strategies will be presented to analyze the successes and limitations of these strategies through a translational lens.

Bioconjugation Insights 2025; 1(4), 109–134 · DOI: 10.18609/bci.2025.023

INTRODUCTION

Nearly all therapeutics, including small molecule, nucleic acid, and protein-based modalities, face delivery challenges. These challenges include, but are not limited to, poor solubility, aggregation, susceptibility to binding by serum proteins and degradation by proteases, inability to permeate cell membranes, sub-optimal trafficking within cell to the site of therapeutic action, non-specific delivery, and off-target cytotoxicity. Therefore, successful clinical translation of any therapeutic requires an accompanying delivery strategy to address these issues.

While there are a plethora of delivery methods in the field, nanoparticle delivery of therapeutics has grown into a rapidly advancing delivery modality with the widespread success of lipid nanoparticle (LNP) packaged-mRNA SARS-CoV-2 vaccines. Recently, polymeric nanoparticles, defined broadly as any particle in the 1–1000 nm range that is primarily composed of polymeric material, have garnered increasing interest, as they have a longer shelf life relative to lipid nanoparticles and can be modified with more ease due to the greater number of functional groups and available ligand conjugation reactions. Their versatility and stability position them as

promising candidates for next-generation drug delivery platforms [1].

Nanoparticles can deliver their encapsulated therapeutic cargo into cells to drug intracellular targets. In broad terms, this intracellular delivery occurs through a cellular process called endocytosis, where a cell engulfs the nanoparticle with its plasma membrane and forms a vesicular sac within itself called an endosome that contains the nanoparticle [2]. The endosome will eventually fuse with lysosomes containing acid hydrolases and other hydrolytic enzymes, and the nanoparticle and its encapsulated cargo will get degraded unless it can escape into the cytosol prior to lysosomal degradation **(Figure 1)**.

It is widely agreed that a primary bottleneck in polymeric nanoparticle-based drug delivery is the process of endosomal escape [3]. Because most therapeutic cargoes aim to drug cytoplasmic or nuclear targets, endosomal escape into the cytoplasm is required for efficacy. However, in the absence of adequate endosomal escape moieties, cargo release is thought to only occur through spontaneous and transient interactions with the endosome's lipid bilayer [4]. Consequently, in a typical nanoparticle, only 1–2% of cargo effectively escapes the endosome [5,6], implying that 98–99% of the delivered therapeutic remains trapped in the endosome and is wasted. Cellular uptake by itself, hence, does not guarantee successful therapeutic delivery, as nanoparticles may readily enter cells without reaching the cytosol. Therefore, successful intracellular delivery requires successful endosomal escape. Here, we outline strategies towards ensuring endosomal escape and cytoplasmic delivery of small molecule, oligonucleotide, and protein drugs. We explore polymer, small molecule, and peptide-based delivery

FIGURE 1

Mechanisms of endocytosis of a model nanoparticle.

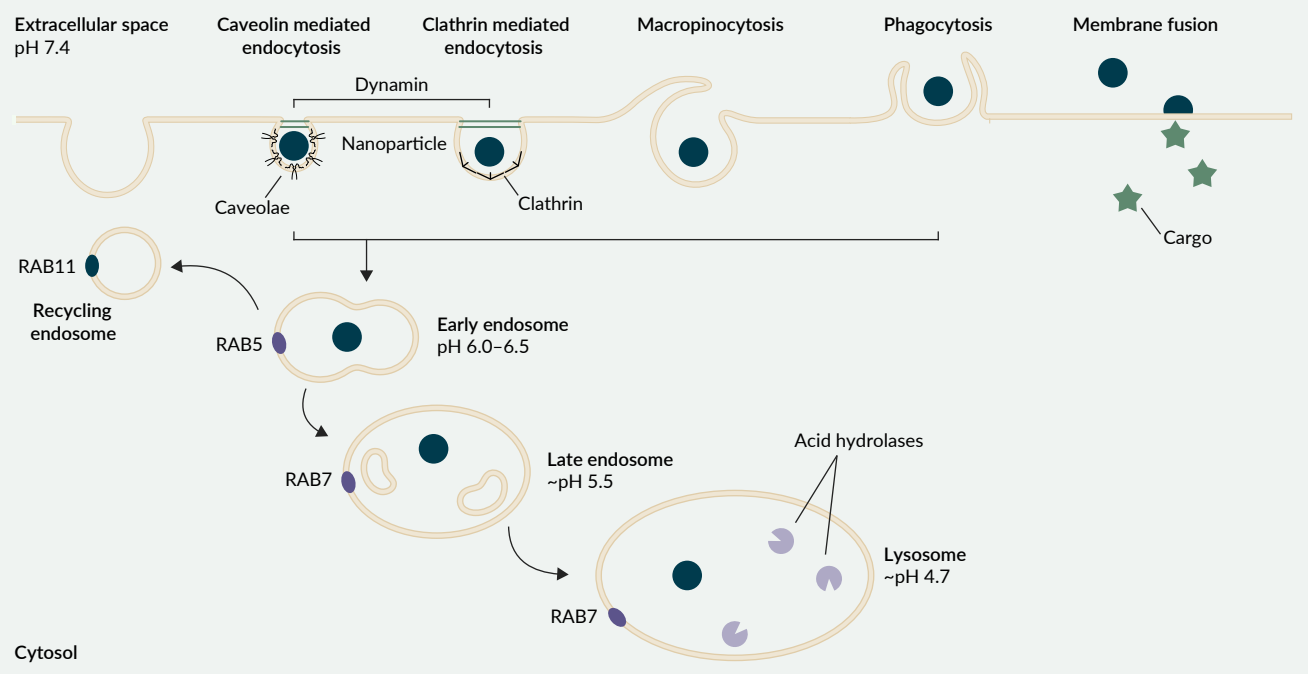

Nanoparticles can be taken up through caveolin or clathrin-mediated mechanisms, macropinocytosis, phagocytosis, or through direct fusion with the membrane; they are then fused to early endosomes, trafficked to late endosomes, and ultimately degraded by acid hydrolases in lysosomes.

systems that are designed to increase endosomal escape, with an emphasis on strategies that are compatible with polymeric nanoparticles **(Table 1)**.

CELLULAR UPTAKE MECHANISMS OF NANOPARTICLES

Understanding endocytosis is imperative to understanding endosomal escape, as nearly all nanoparticles undergo the endosomal-lysosomal pathway once internalized. Endocytosis encompasses both phagocytosis, the uptake of larger particles such as bacteria, and pinocytosis, which internalizes fluids and smaller solutes. Following uptake, nanoparticles are trafficked into early endosome compartments located near the plasma membrane. These early endosomes are marked by RAB5, and exhibit a mildly acidic pH of 6.0–6.5 [7]. Early endosomes function as sorting organelles: while most mature into late endosomes, a subset recycles cargo back to the cell surface through recycling endosomes, identified by the marker RAB11 [8].

Early endosomes then mature into late endosomes, a transition characterized by the exchange of the RAB5 marker protein for RAB7 and the conversion of the phosphatidylinositol (PI) protein PI(4,5)P_2 into PI(3,4)P_2 [8]. This process is accompanied by increased proton influx, and a lowered pH of ~5.5; the acidification process here is leveraged by many pH-responsive endosomal escape moieties to induce endosomal escape, as discussed in later sections. Late endosomes also contain intralumenal vesicles (ILV), which silence signaling receptors and recruit cytosolic proteins through microautophagy, a cellular process where a cell directly engulfs and degrades its own cytoplasmic components [8]. They are additionally enriched in LAMP1 and acid hydrolases that hydrolyze and degrade internalized cargo. Eventually, late endosomes fuse into the highly acidic and degradative lysosomal compartments within the cell; by then, the cargo is typically completely degraded.

The mechanism of nanoparticle internalization varies significantly depending on particle size, charge, and ligand presentation. Nanoparticles can enter cells via multiple endocytic routes, including clathrin-mediated endocytosis (CME), fast endophilin-mediated endocytosis, caveolae-mediated endocytosis (CvME), clathrin-independent carrier endocytosis, and macropinocytosis [9]; among these, CME, CvME, and macropinocytosis are most commonly implicated in nanoparticle uptake.

In clathrin-mediated endocytosis (CME), clathrin-coated pits form on the cell surface upon ligand-receptor activation. These pits rapidly invaginate and, with the help of dynamin, bud into ~120 nm vesicles that internalize the particle [6,7]. CME is the predominant uptake mechanism for many nanoparticles, including polyethylene glycol-polylactide (PEG-PLA) and poly(-lactic-co-glycolic acid) (PLGA) nanoparticles, two of the most common polymeric nanoparticle formulations used for drug delivery [10].

Caveolae-mediated endocytosis (CvME) is another dynamin-dependent endocytosis mechanism in which caveolin, a hairpin-shaped protein, forms cup-shaped invaginations on the cell surface that pinch off into 60–80 nm vesicles. These vesicles then fuse into intermediate caveosomes or ordinary endosomes [10]. CvME has been reported to endocytose primarily smaller nanoparticle formulations like Doxil® and Abraxane®, used clinically to deliver small molecule cancer drugs like doxorubicin and paclitaxel. However, CvME is less prevalent than CME, and is primarily found on endothelial cells [11,12]. Its role in nanoparticle uptake has been questioned, particularly regarding the existence of caveosomes as distinct intermediates in endocytosis [13]; regardless, recent studies still maintain CvME as a form of endocytic uptake of nanoparticles.

TABLE 1

Summary of discussed polymeric nanoparticle-compatible strategies to induce endosomal escape.

Synthetic strategy	Delivery vehicle	Cargo	Endosomal escape mechanism	Reference
Cationic polymers	Esterified PEI polyplex	DNA	Proton sponge effect	[38]
	Disulfide crosslinked PEI polyplex	DNA	Proton sponge effect	[40]
	PEI-fluorocarboxy phenyl boronic acid (FBPA) micelle	siRNA	ATP-mediated disassembly	[43]
	PEG-PBAE nanoparticle (NP)	DNA	Proton sponge effect	[48]
	PBAE-DSPE-PEG core shell NP	mRNA	Proton sponge effect	[49]
	Highly branched PBAE polyplex	mRNA	Proton sponge effect	[50]
	PEG-PACE polyplex and NP	DNA, siRNA, mRNA	Proton sponge effect	[53]
pH responsive polymers	PMPC-DPAEMA polymersomes	DNA	Proton sponge effect	[67]
	PEG-(DMAEMA-co-BMA) polyplex	siRNA	Proton sponge effect	[68]
	PEGMA-DEAEMA-BMA polyplex	mRNA	Proton sponge effect	[69]
	PEG-(DMAEMA-co-BMA) vesicle	Peptide neoantigen	Proton sponge effect	[70]
	DEAEMA-MMA, PEGDMA-AEMA core shell NP	Ovalbumin	Swelling	[71]
	PEG-PBA, DPAEMA-DEAEMA core shell NP	N/A	Swelling	[72]
	Quaternized cationic polycarbonates	DNA	Membrane fusion	[75]
	DMAEMA-b-DMAEMA-BMA-PAA micelle	siRNA	Membrane fusion	[76]
	PEG-b-C7A NP	Tumor antigen	Proton sponge effect	[78]
	Imidazole-conjugated poly(lysine) NP	DNA	Proton sponge effect	[79]
	Histidine substituted poly(lysine) polyplex	DNA	Proton sponge effect	[80]
	PEG-imidazole NP	SN-38	Proton sponge effect	[81]
	polyhistidine-PEG, DSPE-PEG micelle	Paclitaxel	Proton sponge effect	[82]
Small molecule-based	ecoLNP (chloroquine-like LNP)	mRNA	Proton sponge effect	[59]
	Tannic acid-loaded LNP	mRNA	Proton sponge effect	[60]
	Calcium acetate-loaded liposome	SN25860	Proton sponge effect	[61]
	UNC2383, codelivered with therapeutic cargo	SSO, ASO	Pore formation	[63]
	CMP05 and CMP05-7, codelivered with therapeutic cargo	siRNA	Pore formation	[64]
	Silica NP, indocyanine green dye	siRNA, miRNA	Reactive oxygen species generation	[62]
Cell penetrating peptides	Histidine-switching CPP (hsCPP)	Protein	Pore formation	[106]
	Glutamate-modified m-lycotoxin	Protein	Pore formation	[107]
	Spherical nucleic acids	ASO	Pore formation	[108]

TABLE 1 CONT.)

Summary of discussed polymeric nanoparticle-compatible strategies to induce endosomal escape.

Synthetic strategy	Delivery vehicle	Cargo	Endosomal escape mechanism	Reference
Cell penetrating peptides (cont.)	D-penetratin, codelivered with therapeutic cargo	Insulin	Pore formation	[111]
	Chitosan, polaxamer 407, and PEG-modified PLGA NP	Coumarin dye	Pore formation	[114]
	PAMAM dendrimer	Methotrexate	Pore formation	[115]
	Liposome	Mitoxantrone	Pore formation	[116]
Combinatorial strategies	Mannose ethyl methacrylate (ManEMA)-b-DPAEMA-co-PDSEMA	Peptide antigen	Pore formation, proton sponge	[117]
	Elastin-like polypeptide (ELP) micelle	mRNA, DNA, protein	Pore formation, proton sponge	[30]
	Poly(propylacrylic acid) (PPAA) polyplex	Peptide	Pore formation	[119]

Unlike clathrin and caveolin-dependent mechanisms of cellular uptake, macropinocytosis is a dynamin-independent process. Here, folds of plasma membrane extend out from the cell to engulf extracellular material, forming a larger vacuole that can reach up to micron-scale dimensions. Macropinocytosis is less well characterized in the context of nanoparticle internalization; however, it is generally associated for the uptake of larger nanoparticles [14].

The distinct vesicle sizes generated by different uptake mechanisms impose size constraints on nanoparticle internalization, making nanoparticle dimension a key determinant of the route of cellular entry. For instance, a study by Huang and coworkers observed uptake of smaller silica nanoparticles through CvME but little to no uptake of larger silica nanoparticles, likely due exceeding the size threshold for caveolin-mediated uptake [15]. In general, CME and CvME tend to internalize nanoparticles smaller than 200 nm, while macropinocytosis accomodates those larger than 200 nm [9].

Ligand selection further influences the endocytic pathway. For instance, CME has been shown to internalize nanoparticles modified with mannose-6-phosphate, transferrin, riboflavin, and nicotinic acid, while CvME can endocytose nanoparticles whose surface is modified with folic acid or low-density lipoprotein [16]. In fact, the targeting ligand can be even more consequential on the endocytosis pathway a nanoparticle takes than the nanoparticle's properties itself. Gabrielson and Pack demonstrated that polyethylene imine polyplexes were able to undergo both clathrin and caveolae-mediated endocytosis simply by changing the attached ligand: folic acid ligands targeted the caveolar pathway, while transferrin targeted the clathrin pathway [17,18]. Upon blocking each endocytosis pathway individually, they found that blocking CvME affected downstream transfection efficiency significantly more than CME [19]. These results clearly show that the internalization pathway a nanoparticle takes is highly dependent on the context in which it interacts with the cell.

While endocytosis is the dominant route for nanoparticle entry, certain formulations may bypass this pathway entirely by directly fusing with the plasma membrane to deliver cargo into the cytosol. A study by Lu and coworkers demonstrated siRNA-loaded lipoplexes retained their ability to enter cells and silence gene expression even when clathrin, caveolin, and lipid raft-mediated endocytosis pathways were inhibited, thereby suggesting

an endocytosis-independent mechanism of entry was occurring, likely membrane fusion [20]. Recently, several reports have been published reporting that polymeric nanoparticles, when sufficiently small, are able to penetrate through cell membranes and directly access the cytosol [21–23]. However, all of these nanoparticles are 5–10 nm in diameter, and thus the types of therapeutic cargoes that polymeric nanoparticles can deliver through membrane fusion is severely limited.

LIMITATIONS & INNOVATIONS IN QUANTIFYING ENDOSOMAL ESCAPE

Measurement of endocytosis in the context of endosomal escape has proven difficult to standardize due to inherently indirect nature of most assays. Dye leakage assays, commonly using calcein, are frequently employed to qualitatively monitor endosomal escape. At high concentrations and under the acidic conditions of the endosome, calcein fluorescence is quenched; however, upon endosomal escape, the dye disperses into the less acidic cytosolic environment, where it fluoresces, thereby serving as a proxy for escape. A key advantage of calcein leakage assays is their simplicity, as they require no additional modification to the cargo to test. However, the readout of endosomal escape is indirect: a positive calcein signal does not necessarily indicate that the therapeutic cargo has escaped; indeed, false positives are common, as calcein itself can leak from the endosome independently of cargo release [24].

To specifically assess endosome membrane disruption as a proxy to endosomal escape, galectin-based assays have been developed that use fluorescently-tagged galectin to visualize endosomal damage. Upon rupture, fluorescent galectin proteins bind to glycosylated domains on the inner leaflet of the endosomal bilayer, producing localized areas of fluorescence into cells where cargo has escaped [25]. However, galectin binding does not directly confirm cytosolic delivery of cargo, and thus remains an indirect measure.

To this end, more direct quantification methods have emerged. Split-protein complementation assays, such as GFP complementation assays and Split Luciferase Endosomal Escape Quantification (SLEEQ) assays, enable detection of both endosomal damage and successful cytosolic delivery of cargo. These complementation assays rely on transfected cell lines expressing one fragment of GFP or luciferase, respectively, while the complementary fragment is covalently attached to the cargo. Upon endosomal escape, the two fragments of the fluorescent protein reassemble in the cytosol, restoring fluorescence or luminescence. SLEEQ assays, while similar to GFP complementation assays, offer higher sensitivities [26]; however, both assays require transfected cell lines and fragment-conjugated cargo, limiting widespread adoption. Thus, in the field, a tradeoff still exists between assay simplicity and precision of endosomal escape measurement.

COMMON POLYMERIC NANOPARTICLE ARCHITECTURES

The broad category of polymeric nanoparticles can be subdivided into several different nanoparticle architectures, where the architecture that is accessed is dictated by the design of its constituent polymer units. Each of these nanoparticles have differing properties, including size, hydrophobicity, density, and surface charge, which in turn influence the optimal strategies for engineering endosomal escape. Therefore, the choice of endosomal escape mechanism must be tailored to the specific nanoparticle subtype.

Micelles are the most common polymeric nanoparticles for drug delivery. They are typically composed of diblock or triblock block copolymers containing both

hydrophobic and hydrophilic blocks; when these block copolymers are assembled, the resulting micelle has a hydrophobic core and a hydrophilic shell, which solvates and stabilizes it in aqueous environments. Micelles are typically 20–60 nm in diameter, and their hydrophobic core makes them suitable for encapsulating hydrophobic cargo such as small molecule drugs. Although micelle-mediated delivery of macromolecular cargo is typically limited by size, studies have demonstrated successful loading and delivery of DNA, siRNA, and mRNA [27,28]. Poly ethylene glycol (PEG) is frequently used as the hydrophilic block to enhance circulation time and bioavailability of the micelle *in vivo*, resulting in widely studied block copolymers like PEG-PLA (poly[lactic acid]), PEG-PLGA (poly[lactic-co-glycolic acid]), and PEG-PPS (poly[propylene sulfide]).

For nucleic acid delivery, particularly in cellular transfection applications, polyplexes are commonly employed. These nanoparticles form through electrostatic complexation between highly charged—often cationic—polymers electrostatically bind to negatively charged nucleic acids or polymers. Complexation achieves two critical functions: first, it neutralizes the negative charge, as cells do not efficiently internalize negatively charged macromolecules or nanoparticles; second, complexation protects nucleic acids from degradation by nucleases *in vivo* [29]. However, despite charge neutralization, polyplexes often pose toxicity concerns once delivered *in vitro* or *in vivo*.

Larger polymeric nanoparticles are capable of encapsulating bulkier macromolecular cargoes such as mRNA or proteins. Polymersomes—polymeric vesicles with an aqueous core and a hydrophobic bilayer membrane—are formed from diblock or triblock copolymers, and when assembled, form vesicles that are 50–200 nm in diameter. These vesicles can encapsulate larger hydrophilic macromolecules inside the aqueous core, or hydrophobic drugs within their membrane. Another common architecture is the 'micelle-like' core-shell nanoparticles. Core-shell nanoparticles maintain the same hydrophobic core and hydrophilic solvation shell structure as micelles in solution, but are composed of two separate polymer components: an amphiphilic block copolymer and a hydrophobic homopolymer, the latter forming the core. Core-shell nanoparticles are generally larger than micelles at around 100–200 nm in size and thus can accommodate larger macromolecules like mRNA or proteins [30,31].

Given the diversity of nanoparticle architectures, the choice of endosomal escape strategy must be matched to both the nanoparticle design and the modality of the escape agent. Permanently cationic polymers, for instance, are best suited for polyplex formulations, while cell penetrating peptides (CPPs) are more easily conjugated to block copolymers that assemble into micelles or polymersomes. Each strategy also differs in its mechanism of inducing endosomal escape, which depends on the physicochemical properties of the escape agent and its mode of incorporation into the nanoparticle. We will organize strategies by modality and examine the mechanistic rationale behind each successful example. Our discussion will include cationic polymers and endosomolytic small molecules, which share similar mechanisms of endosomal escape, as well as stimuli responsive polymers and cell penetrating peptides.

CATIONIC POLYMER STRATEGIES FOR ENDOSOMAL ESCAPE

Polymers that are cationic at physiological pH have demonstrated the ability to enable cytosolic delivery and endosomal escape of therapeutic cargoes, most commonly nucleic acid cargoes, when internalized. Polyplexes of polymers like poly(ethylene

imine) (PEI) and poly-lysine contain positively charged amino groups that electrostatically complex with the nucleic acids negatively charged phosphate backbone **(Figure 2)**. Once endocytosed, these positive charges in the polyplexes can induce endosomal escape through a mechanism termed the proton sponge effect. As endosomes are acidic, an endocytosed cationic polymer acts as a 'sponge' within the endosome to absorb free protons. This influx in protons is linked with an influx of chloride ions, which act to restore the endosome's equilibrium potential; altogether, this leads to heightened osmotic pressure within the endosome, causing it to swell and eventually rupture **[32]**. While the endosomal buffering from the proton sponge effect is widely held as the primary mechanism of endosomal escape, it is insufficient as a complete explanation as there have been reports suggesting that cationic polymers like PEI do not change lysosomal pH when internalized **[33]**. Therefore, it is likely that cytosolic release can be caused through other mechanisms. The validity of the proton sponge hypothesis will be further discussed in the following section.

Cationic polymers like PEI are still commonly used as part of lipoplexes or polyplexes to complex nucleic acids and proteins **[34]** but are toxic to cells. This is because the exposed cationic amines of unbound PEI can interact with and permeabilize cell membranes, while cargo-bound PEI can cause increased cellular stress and alter the cell's transcriptional processes once delivered **[34,35]**. There are likely several reasons for the toxicity of PEI in comparison to other polymeric nanoparticle formulations, including PEI's resistance to biodegradation once internalized in the cell and particularly high charge density **[34,36]**. Although PEI polyplexes are useful to deliver nucleic acids for *in vitro* applications, they have limited utility *in vivo* because of their toxicity **[37]**.

PEI can be modified to improve the cell viability of the polymer and thereby decrease its toxicity. One approach is to introduce biodegradable moieties into the polymer so that intracellular enzymes can break PEI down, thereby decreasing its toxicity once internalized. One example of this approach is to introduce ester bonds into PEI segments that cells can hydrolyze easily **[38]**. Another approach leverages the

FIGURE 2

Representative structures of polymers and small molecules used for endosomal escape.

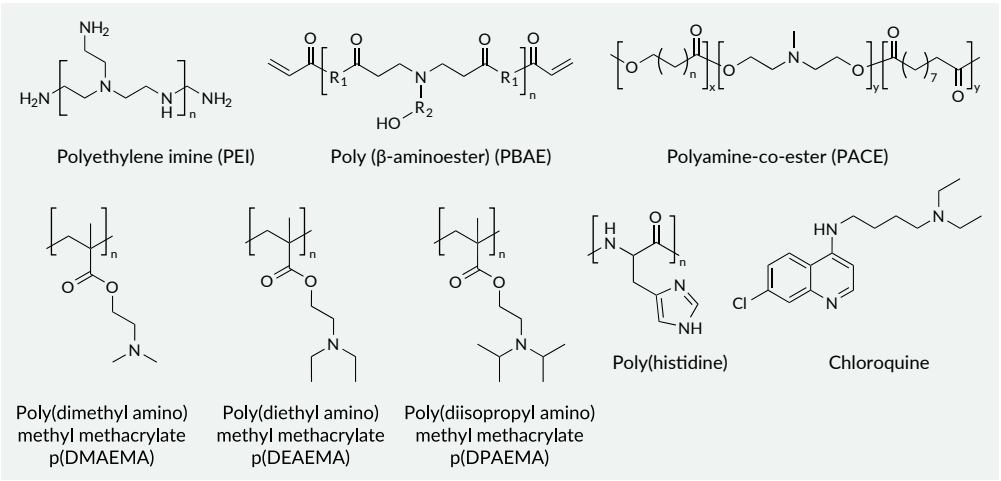

endosome's highly reductive environment by conjugating short thiolated PEI fragments together to make disulfide linked-PEI, which can be reduced and degraded by enzymes like glutathione or glutathione reductase that are found at much higher concentrations within the cell [39,40].

However, the simplest and most commonly used method of minimizing cytotoxicity is to use shorter PEI segments, even though polyplexes composed of lower molecular weight polycations have been shown to negatively impact the stability of the polyplex [41,42]. To this end, shorter PEI segments can be combined with hydrophobic blocks in core-shell nanoparticle formulations to increase their stability while still retaining their less cytotoxic properties to elicit productive endosomal escape. For example, Zhou *et al.* developed a PEI-based nanoparticle platform for siRNA delivery by grafting low molecular weight (LMW) PEI to a hydrophobic cholesterol core that lowered the toxicity in comparison to a higher molecular weight PEI polyplex control; furthermore, this nanoparticle platform was able to demonstrate effective endosomal escape through an endosomal ATP-dependent mechanism [43] .

Poly(ß-aminoesters) (PBAE) are another class of cationic polymer that have been preferentially used over PEI for nucleic acid delivery [44]. The synthesis of PBAE is more modular than PEI, as PBAE is polymerized in a stepwise fashion with two different monomers—a diacrylate and an amine—that can be combined to make a variety of different PBAE polymers. As a result, libraries of PBAE can be made and screened, allowing for the identification of PBAEs with the highest encapsulation and transfection efficiency, or the least cytotoxicity [45,46]. Routkevitch *et al.* found that the transfection efficiency of PBAEs was limited by endosomal escape, not cell uptake, and that successful endosomal escape was reliant on the pKa of the PBAE polymer, where the most effective PBAEs had a pKa that fell within the endosomal pH range [47].

PBAE nanoparticles are effective gene delivery vehicles for *in vivo* applications. A recent study screened a library of polyethylene glycol (PEG)-coated PBAE nanoparticles to identify those that exhibited high stability, transfection efficiency, and cell viability [48]. The optimal nanoparticle formulation was then loaded with a suicide gene therapy, delivered in a preclinical orthotopic human model of glioblastoma, and showed a 25% increase in median survival. Another study used a lipid-coated PBAE nanoparticle for cytosolic delivery of mRNA [49]. Endosomal escape was quantified by a calcein dye release assay that compared the lipid-coated PBAE nanoparticle to a lipid-coated PLGA nanoparticle control, and it was found that the PBAE core endowed the platform with endosomal escape capabilities. This was used to deliver mRNA intranasally, which has potential future applications for the noninvasive delivery of mRNA vaccines. Recently, a study by Yong *et al.* also screened through a library of highly branched PBAEs with variable degrees of branching, polymer structures, and terminal amine end-groups to find effective PBAE polyplexes for mRNA delivery [50]. When delivered *in vivo*, the choice of the terminal amine at the surface of the polyplex targeted different organs for delivery; polyplexes with terminal morpholine groups were able to bias mRNA delivery to the liver, while polyplexes with terminal ethylenediamine groups targeted delivery to the spleen.

Poly(amine-co-ester) (PACE) are another category of biodegradable cationic polymers. PACE was designed to have a lower charge density than PEI, and biodegradable ester bonds along its polymer backbone to reduce its cytotoxicity compared to PEI as well. Because of its lower charge density, electrostatic interactions between the polymer and the DNA are likely not sufficient to completely condense

nucleic acids into the polyplex; however, PACE polymers are more hydrophobic than PEI, which can strengthen hydrophobic interactions between the polymer and the phospholipid membranes of the endosome and help increase endosomal escape through membrane fusion [51]. Indeed, when loaded with DNA for *in vitro* delivery, both the cell viability and transfection efficiency of PACE polyplexes outperformed that of standard transfection reagents like PEI and Lipofectamine™ [52]. The synthesis of PACE is also modular, similarly to PBAE, which has been to screen and identify candidates that were able to effectively deliver plasmid DNA, siRNA, and mRNA [53]. Most recently, Suberi *et al.* used PACE polyplexes to effectively facilitate intranasal delivery of mRNA encoding the SARS-CoV-2 spike protein, highlighting their potential application as a delivery platform for inhalable mRNA vaccines [54].

SMALL MOLECULE-BASED APPROACHES

Small molecules are an alternative approach to induce endosomal escape. Chloroquine, a small molecule drug that is traditionally used as a treatment for malaria, was the first small molecule that was shown to induce effective endosomal escape through the proton sponge effect [55]. It is weakly basic and capable of protonating its tertiary amine at the endosomal pH range; furthermore, it contains hydrophobic aromatic ring motifs that interact with the endosomal membrane and encourage rupture [4,56]. Chloroquine can be delivered alongside polymeric nanoparticles through simple co-delivery with the cargo or incorporated into polymers with custom monomers [57,58]. However, chloroquine is highly cytotoxic, especially at the concentrations required for effective endosomal escape, so that its use as an endosomolytic agent is limited to *in vitro* applications only.

To address the issue of chloroquine's cytotoxicity, a recent study screened for chloroquine-like small molecules that were directly conjugated onto an ionizable lipid and could retain chloroquine's endosomolytic behavior within the LNP but with reduced cytotoxicity [59]. A library of chloroquine-like lipids was generated by varying the structure of its three modular segments—the quinoline ring scaffold, the ionizable linker, and the lipid tail. The leading ionizable lipid candidate was identified through Central Composite Design, a powerful optimization methodology, and the resulting LNP elicited effective endosomal escape and delivered significantly higher levels of mRNA *in vivo* than the clinically approved LNP formulation distributed by Moderna. Another paper by Ma and Fenton used the polyphenols as a chloroquine substitute for endosomal escape. Tannic acid was chosen as the candidate polyphenol, as it contains the appropriate aromatic rings and phenolic hydroxyl groups that have been hypothesized to be the key motifs driving endosomal escape; it is also well tolerated in the body, as it is generally recognized as safe (GRAS) by the FDA and is commercially available. Tannic acid was incorporated directly into the membrane of a lipid nanoparticle platform without prior conjugation to any lipid component, simply by including the tannic acid molecule in the ethanol phase during microfluidic mixing and LNP formulation. The resulting tannic acid-loaded LNP was then applied to deliver mRNA payloads. It significantly improved endosomal escape compared to LNPs loaded without tannic acid, as evaluated by confocal microscopy of fluorescently labeled LNPs, and exhibited minimal cytotoxicity [60].

Other small molecules unrelated to chloroquine have also been shown to help induce endosomal escape. For instance, Yang and coworkers used calcium acetate to remotely load small molecule drugs into a liposome by establishing a transmembrane

gradient across the lipid membrane; subsequently, the calcium ions were also able to increase endosomal rupture through the proton sponge effect [61]. Wang and coworkers also achieved *in vivo* suppression of tumor growth with a combination of miRNA and siRNA delivering them with a light responsive indocyanine green dye silica nanoparticle conjugate. Here, the indocyanine green was able to generate reactive oxygen species in response to light, which induced endosomal rupture [62]. Another study by Wang and coworkers screened several small molecule libraries and identified a small molecule compound, UNC2383, which improved cytosolic release of antisense oligonucleotides and splice switching oligonucleotides (SSO). However, while its toxicity is lower from chloroquine, the therapeutic index of UNC2383 is still too narrow to be useful *in vivo* [63]. Recently, UNC2383 was used as a starting point to identify two new compounds, CMP05 and CMP05-7, which had comparable increase in SSO activity *in vitro* to UNC2383, and effective endosomal escape [64].

While most of these small molecules for endosomal escape are hypothesized to induce endosomal rupture through the proton sponge effect, similarly to cationic polymers like PEI, the validity of the proton sponge hypothesis as a mechanism for endosomal escape is still widely debated [65]. Several studies experimentally support the existence of the proton sponge effect [51,66]; however there have also been studies that argue that the proton sponge effect is not sufficient to induce endosomal escape and suggest that other features of effective endosomolytic moieties likely aid in endosomal escape through alternate mechanisms, such as membrane fusion or nanoparticle swelling [33,65]. These alternate mechanisms have since been incorporated into the design of polymer nanoparticles for endosomal escape, as discussed in the following section.

DESIGN PRINCIPLES OF pH RESPONSIVE POLYMERS FOR CYTOSOLIC DELIVERY

In the endosomal/lysosomal pathway, the pH in the endosome drops from the physiological pH of 7.4 to 6.0–6.5, then even lower to ~5.0 in the lysosome [14]. As such, pH responsive polymers have become effective approaches that leverage the low pH of endosomes to trigger endosomal escape, in contrast to PEI and chloroquine that stay protonated throughout endocytosis. The strategy by which pH responsive polymeric nanoparticles aid in endosomal escape, in addition to the proton sponge effect that occurs once protonated, is dependent on the material **(Figure 3)**. One proposed strategy of endosomal escape is through the build-up of osmotic pressure within the endosome through pH-triggered nanoparticle dissolution. Upon endocytosis, the low pH of the endosomes triggers the polymers to protonate, which results in the nanoparticle disassembling into its constituent polymer chains, creating increased osmotic pressure within the endosome and eventually helping to rupture the endosome [67]. This mechanism was first proposed when pH sensitive polymersomes of a block copolymer with a hydrophobic poly(diisopropylamino) ethyl methacrylate (DPAEMA) block were observed through dynamic light scattering (DLS) to dissociate into their unimer components at endosomal pH and enable cytosolic delivery of fluorescent dye cargoes [67]. The effective cytosolic delivery of siRNA has also been reported in a PEGylated polyplex of dimethylamino ethyl methacrylate-co-butyl methacrylate (DMAEMA-co-BMA) copolymers, which was observed to dissociate at endosomal pH and facilitate siRNA and mRNA delivery *in vitro* and *in vivo* [68,69]. Nanoparticles of this polymer have been used to deliver peptide-based cancer antigens to vaccinate against a colon carcinoma model *in*

FIGURE 3

Schematic of mechanisms capable of inducing endosomal escape.

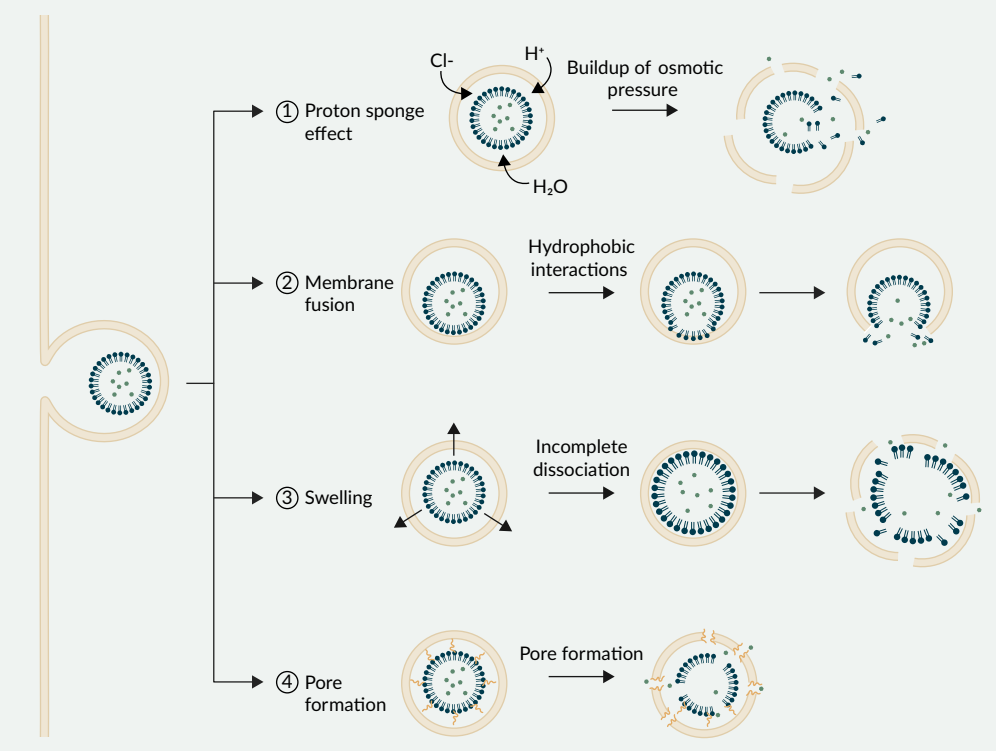

Endosomes can be ruptured through the proton sponge effect through osmotic pressure buildup; fused with the hydrophobic endosomal membrane to facilitate release of cargo; exert pressure on the endosomal cavity as a result of incomplete dissociation to induce rupture; or punctured by pore formation with CPPs.

vivo, significantly delaying tumor growth and improving survival [70].

Polymer nanoparticles can also exert pressure upon the endosomal membrane by swelling. pH responsive polymers will protonate and dissociate at endosomal pH; however, if a nanoparticle is designed such that it cannot disassemble, it will instead swell in size. This strategy was utilized by Hu *et al.*, where they designed a core-shell polymer nanoparticle with a hydrophobic core consisting of the pH-sensitive polymer block of poly(diethylamino ethyl methacrylate) (DEAEMA) and a hydrophilic poly(ethylene glycol) dimethylacrylate block. The polyDEAEMA core was then crosslinked to prevent the nanoparticle from dissociating once protonated, and as endosomal pH was reached, these nanoparticles swelled to 2.8 times their original diameter. Effective endosomal escape was also seen through confocal microscopy, and these nanoparticles were capable of effectively delivering a protein cargo—ovalbumin [71].

However, recently a study by Kermaniyan *et al.* reported that a similarly swelling nanoparticle led to no endosomal escape [72]. In this paper, although nanoparticles were synthesized with similar DEAEMA component as the study by Hu and coworkers [71], there were different mechanisms of withholding complete dissociation to induce swelling. While the previous study utilized crosslinking to swell the nanoparticle, this study relied on emulsifying pH sensitive and pH-insensitive components together with no crosslinker, which achieved only up to a two-fold change in diameter. While this difference in swelling could be within experimental error,

it is possible that the amount which their nanoparticles swelled may be insufficient for the critical swelling needed for endosomal rupture, ultimately suggesting that the efficacy of swelling as a mechanism for endosomal escape remains an open area of investigation.

Another strategy of endosomal escape that has been used is through membrane fusion, where components of a nanoparticle merge with the phospholipid membrane of the endosome to release its cargo [73]. This is the putative mechanism of endosomal escape that lipid nanoparticles (LNP) undergo once endocytosed, due to the ionizable lipid component of the LNP favoring a conformation that allows for lipid exchange with the endosomal membrane [74]. While polymeric materials cannot undergo lipid exchange, increasing the hydrophobicity to better match that of the endosomal membrane can facilitate membrane fusion. Indeed, in a study of a polymeric nanoparticle delivering DNA, authors found that an increase in the hydrophobicity of the polymer's side chains increased the delivery and expression of the DNA cargo, indicating that hydrophobicity is a reliant a parameter in the design polymer of polymers for endosomal escape [75].

Another approach employs the pH responsive membrane fusion mechanism by using the PEG-DBP platform, involving PEG, DMAEMA, butyl methacrylate (BMA), and propylacrylic acid (PAA). Here, researchers use PAA as the pH sensitive component, which becomes more hydrophobic at endosomal pH. PAA is copolymerized with a core-forming BMA component and a cationic DMAEMA component, which is then assembled into a core-shell micelle. At physiological pH, the net charge is neutral, which helps to reduce toxicity, but at acidic pH the carboxyl groups of the PAA protonate and neutralize the charge of the polymer, thereby decreasing its ability to solvate with water ions and increasing the overall hydrophobicity of the polymer. Together, the buildup of positive charge from DMAEMA and the ability to fuse with the endosomal membrane endowed by PAA facilitate effective cytosolic delivery of siRNA, leading to knockdown of mRNA expression *in vitro* [76].

It is worth noting that several of these polymeric nanoparticle systems use the same tertiary amines to endow their nanoparticles with pH-responsive behavior. Dimethylamino ethyl methacrylate (DMAEMA), diethylamino ethyl methacrylate (DEAEMA), and diisopropylamino ethyl methacrylate (DPAEMA) are often used as pH-responsive monomers in polymers for endosomal escape because they are readily available and are compatible with controlled radical polymerization techniques for polymer synthesis. All these monomers have the same backbone, with only the tertiary amine's side chains differing between them [77]. However, the complexity of side chains is not limited to only methyl, ethyl, or isopropyl groups. For instance, Luo *et al.* synthesized polymeric micelles from a library of ultra-pH-sensitive (UPS) tertiary amine polymers with linear and cyclic side chains to deliver tumor antigens to cytotoxic T cells for cancer immunotherapy [78]. The leading candidate from this library was a seven membered ring with a tertiary amine, deemed C7A, that protonated at pH 6.9. C7A only dissociated at endosomal pH and elicited a significantly stronger cytotoxic T cell immune response than other formulations, indicating that the side-chain architecture is a significant parameter to consider in the design of polymeric nanoparticles capable of cytosolic delivery of cargo.

Imidazole groups have also been used as pH-responsive moieties in polymeric nanoparticles. Imidazoles are aromatic rings that contain a secondary amine and have a pKa within the endosomal pH range at 6.9. They are also found in histidine, and hence many polymers use a poly-histidine or other imidazole-containing block to

endow nanoparticles with an endosomal pH response. For instance, substituting histidine residues or imidazolacetic acid side chains into the cationic polymer—polylysine—can increase the transfection efficiency of plasmid DNA to levels comparable to PEI, but with significantly decreased cytotoxicity [79,80]. Another study formulated micelles with imidazole side chains and zinc ions that can deliver small molecule chemotherapeutics to tumor cells [81]. Here, the zinc ions coordinate the imidazole groups so that they are unprotonated; once in the tumor cell, the influx of protons displace the coordination bonds and induce endosomal escape through the proton sponge effect. Another study delivered chemotherapeutics by combining PEG-grafted polyhistidine polymers with the phospholipid DSPE to form a mixed polymeric micelle, which exhibited pH dependent release and successful cytosolic delivery of the anticancer small molecule paclitaxel [82].

REDOX & LIGHT-TRIGGERED MECHANISMS OF ENDOSOMAL ESCAPE

pH remains the most reliable and widely exploited stimulus for endosomal escape; however, alternate triggers, though less commonly exploited, have also been used. One such approach leverages high intracellular concentrations of glutathione, a strategy long employed in drug delivery to enable reduction-sensitive delivery of therapeutics. Nanoparticles that are designed for redox response incorporate disulfide bonds into the polymer composition. Once internalized, glutathione cleaves the bonds into free thiols to disrupt the nanoparticle architecture [83].

Beyond cargo release, redox-triggered mechanisms can also be applied to endosomal escape. A recent study demonstrated through confocal microscopy that incorporation of disulfide bonds into nanoparticle architectures can achieve effective endosomal escape and cytosolic release. The disulfide bonds were hypothesized to facilitate endosomal escape through random and non-specific binding to free thiols on the inner layer of the endosomal membrane, thereby causing strain on the endosome and eventually contributing to its membrane rupture [84].

Other external stimuli—including light, ultrasound, and presence of electromagnetic fields—have also been explored for endosomal escape. Among these, photo-activated endosomal escape is the most reported, as light allows for a high level of spatiotemporal control while minimizing tissue damage. In this strategy, nanoparticles are engineered to generate highly disruptive reactive oxygen species (ROS) in response to an external light source, typically through photo activatable moieties such as light-sensitive small molecules or ROS-labile bonds.

For instance, the light-activated siRNA endosomal release (LASER) platform was developed with porphyrin, a molecule found in naturally occurring compounds like hemoglobin and chlorophyll. Porphyrin-conjugated lipids were incorporated into a LNP formulation along with siRNA through microfluidic mixing. Once internalized by cells, these porphyrin-containing LNPs fused with the endosomal membrane, similarly to the hypothesized mechanism of LNP-mediated endosomal escape. Upon light exposure, the porphyrin lipids enhanced generation of reactive oxygen species while buried within the endosomal membrane, inducing endosomal rupture and subsequent cytosolic release of siRNA as confirmed by confocal microscopy and galectin disrupting assays [85].

Another study incorporated ROS-sensitive linkers into an oligoethyleneimine (OEI) polyplex for DNA delivery. The design included an aminoacrylate bond cleavable by a singlet oxygen generated upon light exposure. In addition, the

authors embedded a fluorogen that tracked ROS-directed degradation and endosomal escape through aggregation-induced emission (AIE). When the nanoparticle was internalized yet still intact, the fluorogen moieties were in clustered, producing fluorescence; upon degradation and cytosolic release, the components of the nanoparticle became diffuse within the cytosol and fluorescence was lost. Indeed, effective photo-induced endosomal escape in cells was observed through confocal microscopy after five minutes of radiation from visible light [86].

It is worth noting, however, that while light-based strategies demonstrate effective *in vitro* endosomal escape, this often does not equate to effective *in vivo* endosomal escape. Limited tissue penetration of light into cells *in vivo* is much more challenging, and requires light exposure regimens that are difficult to translate clinically.

PEPTIDE-BASED SOLUTIONS

Cell penetrating peptides (CPPs) have also been used to enable cytosolic delivery of therapeutics (Table 2). CPPs are short peptides of 5–10 amino acids that interact with and penetrate through cell membranes. They generally fall into two categories: cationic and amphiphilic [87]. Cationic CPPs typically contain amino acids like histidine, arginine, and lysine that are positively charged at physiological pH and interact with negatively charged phospholipid membranes in the cell. The most ubiquitous example of a cationic CPP is TAT, the translocating peptide from the Trans-Activator of Transcription protein that is derived from HIV [88]. TAT is perhaps the most commonly used CPP to aid cytosolic delivery, as its ability to translocate through cell membranes when conjugated or co-delivered with the therapeutic of interest has been well characterized in the field [89,90]. However, its efficacy at inducing endosomal escape is low. Penetration through the endosomal membrane requires high concentrations of TAT, and the efficacy of TAT is highly variable depending on the cargo and conjugation mechanism it accompanies [91,92]. Oligo-arginine, a peptide consisting of 8–10 cationic arginines, is

TABLE 2

Summary of discussed CPPs shown to aid in endosomal escape.

Name	Sequence	Class	Reference
TAT	GRKKRRQRRR	Cationic	[88]
R8	RRRRRRRR	Cationic	[93]
HA-2	GLFGAIAGFIENGWEGMIDGWYG	Amphipathic	[94]
PEP-1	KETWWETWWTEWSQPKKKRKV	Amphipathic	[95]
Penetratin	RQIKIYFQNRRMKWKK	Cationic, amphipathic	[104]
LMWP	VSRRRRRRGGRRRR	Cationic	[106]
M-lycotoxin	IWLTALKFLGKHAAKHLAKQQLSKL	Amphipathic	[107]
Aurein 1.2	GGGLFDIIKKIAESF	Amphipathic	[108]
gH625	HGLASTLTRWAHYNALIRAF	Amphipathic	[116]
Melittin	GIGAVLKVLTTGLPALISWIKRKRQQC	Cationic, amphipathic	[117]
S10	KLALKLALKALKAALKLA	Amphipathic	[30]
YARA	YARAAARQARA	Cationic	[118]

another common CPP [93]. The other class of cell penetrating peptides, amphiphilic cell penetrating peptides, form amphipathic helices with a hydrophilic and hydrophobic face. They induce cytosolic delivery of therapeutic cargo through hydrophobic interactions with the phospholipid membrane. Examples of such CPPs include the HA-2 peptide and PEP-1, which have been reported to induce cytosolic release of associated cargo [94,95].

CPPs can escape the endosomal compartment to induce cytosolic delivery by inserting themselves into the endosomal membrane through cationic or hydrophobic interactions, leading to pores in the membrane through which the cargo can be released into the cytoplasm **(Figure 4)**. Alternatively, they can also result in cytosolic delivery through transduction, where the CPP is directly translocated across the plasma membrane into the cytosol and the endosome is bypassed entirely [96]. The mechanism by which endocytosis or transduction occurs can be engineered to some extent: studies have shown that cyclized analogs of both TAT and octa-arginine that are conjugated directly to protein cargo preferentially induce transduction and direct cytosolic delivery [97,98]; however, it is highly dependent on the concentration of the CPP and the payload. Transduction is preferentially induced when concentrations of CPPs are high enough to induce toxicity to the cell, and transduction efficiency decreases with the size of the cargo [92,99,100]. Endocytosis will likely be the primary form of cellular uptake for CPPs that decorate polymeric nanoparticles, and endosomal escape will be favored over transduction for cytosolic delivery.

CPPs have been used to facilitate delivery of cargoes in preclinical studies for the treatment of cancer and diabetes [101,102], but translation into a clinical setting is limited, and no drugs using excipient CPPs have been approved by the FDA. For one, surface bound CPPs lack any targeting moiety, which leads to systemic toxicity as CPPs induce pore formation in membranes of off-target cells [103]. This issue of systemic toxicity is often exacerbated by the need to dose CPPs at high concentrations in order to achieve successful cytosolic release of cargo. Secondly, it is possible that CPPs can induce immunogenicity due to their polypeptide structure, as demonstrated by the CPP penetratin's ability to induce innate immunity *in vivo* [104]. Finally, CPPs have a short half-life, and are easily degradable by proteases and serum proteins before they are endocytosed and enable endosomal escape of their cargo [105].

Because of this, recent studies that use CPPs to induce endosomal escape must often leverage other strategies to address these limitations. For instance, the pH drop in endosomes can be utilized to keep CPPs inert until they are endocytosed. An example of this is the histidine switching CPP (hsCPP) in which the arginine and lysine residues of several common cationic CPPs were mutated to histidines. These hsCPPs are uncharged at physiological pH, but once endocytosed, the histidine residues protonate, and the hsCPP induces endosomal escape of the cargo. The most endosomolytic hsCPP, a histidine switched analog of low molecular weight protamine (hsLMWP), was conjugated to a targeting antibody for increased cellular uptake and a protein cargo of interest, and then evaluated for endosomal escape, effective protein delivery, and immunogenicity. This hsCPP was able to effectively deliver protein cargo both *in vitro* and *in vivo* [106].

Another study mutated the venom-derived peptide m-lycotoxin to reduce non-specific disruption of cell membranes. M-lycotoxin has an amphipathic helix, of which the hydrophobic face interacts with the plasma membrane. The authors hypothesized that a negatively charged glutamate residue on the hydrophobic side of the helix would prevent m-lycotoxin from association

FIGURE 4

Schematic of mechanisms exhibited by CPPs to induce effective cytosolic delivery of conjugated cargo.

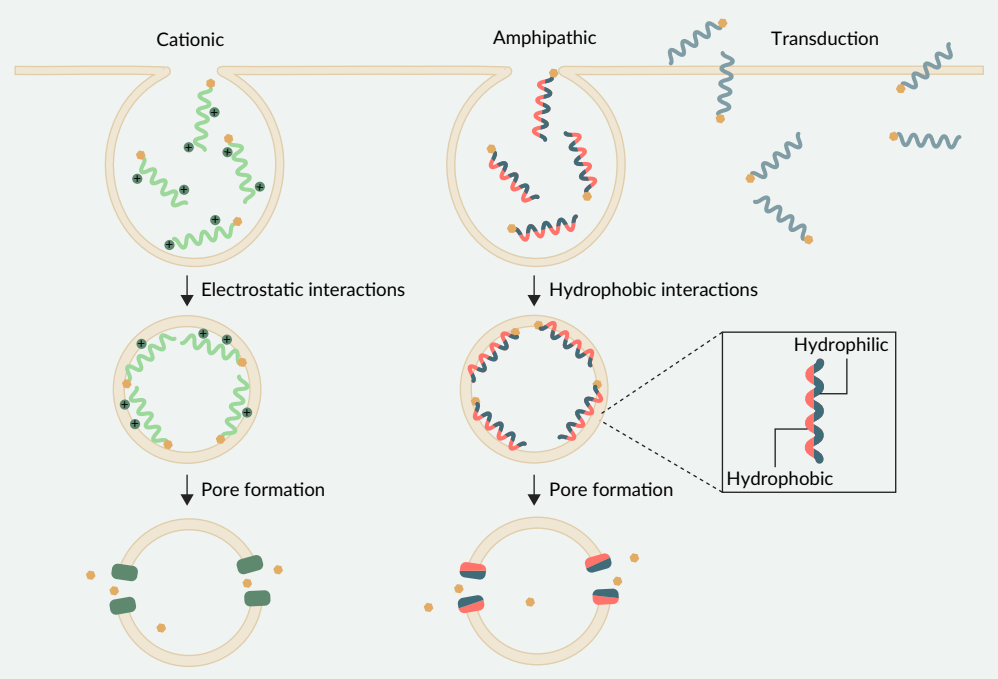

Cationic CPPs and amphipathic CPPs use different properties to interact with the endosomal membrane to insert into the membrane and form pores: cationic CPPs electrostatically interact with the anionic membranes, while the hydrophobic face (red) of amphipathic CPPs fuse to the hydrophobic phospholipids. Certain CPPs can transduce directly across the plasma membrane to deliver their conjugated cargo into the cytoplasm.

with the plasma membrane and therefore be non-lytic. Once endocytosed, the subsequent pH-dependent protonation of glutamate should cause the now neutral CPP to become lytic. However, it was found that the glutamate-modified M-lycotoxin promoted endosomal escape of antibodies and other protein cargoes by an alternative indirect and lipid composition-dependent manner. The glutamate modification of m-lycotoxin acts as a 'safety catch' to prevent the peptide from lysing the plasma membrane but does not impact disruption of the endosomal membrane, thus conferring selective endosomal activity without the typical toxicity of wildtype M-lycotoxin [107].

Strategies to improve the efficacy of CPPs can also be engineered into nanoparticles. Narum and coworkers report a pH-responsive spherical nucleic acid nanoparticle platform, termed the DNA EndosomaL Escape Vehicle Response (DELVR) platform, that is composed of a gold nanoparticle core and a nucleic acid shell that can deliver antisense oligonucleotides (ASOs). Here, the CPP Aurein1.2 is hybridized to the nucleic acid strands that form the corona of the nanoparticle so that it is oriented towards the inside of the DNA shell, closer to the nanoparticle core. Once endocytosed, the DNA shell refolds, which releases the therapeutic ASO and exposes the CPP to the endosome. This allows for effective endosomal escape while avoiding any nonspecific lysing of plasma membranes [108].

CPPs can also be engineered so that they are more resistant to enzymatic degradation. One method of improving stability is to replace the typical L-amino acids used

in peptides with D-conformation amino acids, as D-amino acids are not recognized by metabolic enzymes [109]. Indeed, it was found that the D-conformation of penetratin degraded much slower than the L-conformation and was able to double the half-life of insulin *in vivo* in comparison to D-penetratin [110]. However, while D-amino acids have not been found to be toxic, they are retained for a longer time in the cytoplasm following endosomal escape, which has been seen to impact cell proliferation and transcription [111]. PEGylation of CPPs can also improve their stability and half-life [112]; however, with the emergence of anti-PEG antibodies in recent decades, the stealth behavior that PEG endows to CPPs is likely to decrease [113].

While CPPs are most commonly directly conjugated to a therapeutic protein of interest, CPPs can be bound to polymeric nanoparticles electrostatically or covalently conjugated through a variety of click chemistry reactions. One study electrostatically bound the cationic peptides TAT, octa-arginine, penetratin, and low molecular weight protamine (LMWP) through simple mixing with PLGA nanoparticles, which exhibits a negative surface charge [114]. In another study, a TAT-derived peptide containing a free cysteine thiol group was conjugated to a PAMAM dendrimer nanoparticle functionalized with PEG-maleimide end groups through a thiol-maleimide click reaction [115]. Copper-catalyzed azide-alkyne cycloaddition (CuAAC) has also been used to conjugate the peptide gH625 with an alkyne-containing moiety, to a liposome decorated with PEG-azide [116]. These studies illustrate that CPPs can be attached to polymeric nanoparticles by standard bioconjugation methods.

TRANSLATIONAL INSIGHT

While many endosomal escape strategies enable cytosolic delivery of therapeutic cargo, there are intrinsic limitations that are likely to prevent their commercialization and translation to the clinic. Chief among these is the fine balance between efficacy and cytotoxicity in any endosomal escape strategy: at suboptimal concentrations, escape moieties are ineffective, yet if dosed at high enough concentrations to effectively rupture endosomes, they risk indiscriminately puncturing membranes within the cell or disrupting native cellular machinery. A potential solution to this limitation is to integrate multiple classes of endosomal escape moieties to exploit different mechanisms of cytosolic release to increase endosomal escape efficacy.

This approach was demonstrated with the virus-inspired polymer for endosomal release (VIPER) platform, a micelle platform in which the hydrophobic core is composed of pH-responsive DPAEMA copolymerized with pyridyl disulfide ethyl methacrylate (PDSEMA). The PDSEMA is further covalently conjugated to melittin, a virus-derived CPP. In an extracellular environment, the hydrophobic core of the micelle hides the CPP, preventing it from triggering adverse immunogenicity or cytotoxicity, and once internalized, the drop in pH triggers DPAEMA to protonate and disassemble the micelle. This exposes melittin, which can rupture the endosomal membrane; the disassembled DPAEMA can also synergistically improve cytosolic release, partially by increasing the osmotic pressure within the endosome and partially by triggering the proton sponge effect. The VIPER platform was tested *in vivo* by intraperitoneal administration in a tumor-bearing mouse model, where it slowed tumor growth down and significantly improved survival [117].

A recent study by Eweje and coworkers also demonstrates the complementary combination of pH response and membrane rupture in the elastin-based nanoparticles for therapeutic delivery (ENTER) platform: they developed multiple generations of an

elastin-like polypeptide (ELP) based vesicle and found that by a) enriching the hydrophobic portion of the ELP with histidine residues and b) incorporating endosomal escape peptides such as S10 into the core of the vesicle, they were able to achieve pH-triggered exposure of the peptide and effective endosomal escape. This ELP vesicle enabled efficient delivery of protein, siRNA, and mRNA cargoes, demonstrating the platform's versatility [30].

Evans and coworkers combined CPPs with the polymer poly(propylacrylic acid) (PPAA) into a polyplex that leverages these two synergistic moieties to induce effective endosomal escape. PPAA is hydrophobic and anionic, and once the polyplex is endocytosed, PPAA's hydrophobic backbone fuses with the endosomal membrane. The anionic component of PPAA, which has already been electrostatically bound to the cationic cell penetrating peptide within the polyplex, then anchors the CPP to the endosomal membrane and enhances its ability to rupture the endosome [118]. This PPAA-CPP platform was used to deliver vasoactive peptides to vascular smooth muscle cells to inhibit vasoconstriction, and has also recently been used to deliver other cationic peptide payloads [118,119].

Despite these innovations, clinical translation of endosomal escape technologies remain limited. With the exception of cell penetrating peptides, which have been entered clinical trials as cancer therapeutics but have yet to receive FDA approval [120], most developments in endosomal escape have not progressed beyond preclinical stages. This stagnation primarily reflects the broader lack of clinical advancement of polymeric nanoparticles, rather than fundamental flaws in endosomal escape mechanisms. In general, the drug delivery field bottlenecked by several factors, including poor targeting specificity, inadequate sustained-release profiles, and logistical hurdles in storage and processing [120]. To this end, polymeric nanoparticles offer potential solutions, as their surfaces can be readily engineered for targeted delivery, and recent studies have developed highly thermostable formulations that simplify transport and storage [31,121].

However, polymeric nanoparticles have achieved limited clinical adoption in comparison to other platforms. This is not without exception: several polymeric formulations are FDA approved, including Abraxane (an albumin biopolymer-based nanoparticle for delivery of paclitaxel), Zilretta®, an (PLGA microspheres for extended-release osteoarthritis treatment), and Apretude® (a long-acting injectable for HIV pre-exposure prophylaxis). However, the key barrier to broader integration lies in the incomplete understanding of how polymeric nanoparticles interact with biological barriers, both on the extracellular and intracellular level [122].

This includes a limited grasp of endosomal escape dynamics. Many nanoparticles described here rely on escape agents that are already synthetically accessible through solid-phase synthesis, chemical conjugation, or recombinant expression, thereby making them scalable and manufacturable. However, without rigorous evaluation of their safety profile in humans, these platforms will remain limited to preclinical use. Therefore, while significant progress has been made to overcome the challenge of endosomal escape, further innovation is still required to pave the way for polymeric nanoparticles to fully translate to the clinic and become the next innovation in drug delivery.

REFERENCES

1. Lu H, Zhang S, Wang J, Chen Q. A review on polymer and lipid-based nanocarriers and its application to nano-pharmaceutical and food-based systems. *Front. Nutr.* 2021; 8, 783831.
2. Banushi B, Joseph SR, Lum B, Lee JJ, Simpson, F. Endocytosis in cancer and cancer therapy. *Nat. Rev. Cancer* 2023; 23, 450–473.
3. Shete HK, Prabhu RH, Patravale VB. Endosomal escape: a bottleneck in intracellular delivery. *J. Nanosci. Nanotechnol.* 2014; 14, 460–474.
4. Dowdy SF. Endosomal escape of RNA therapeutics: how do we solve this rate-limiting problem? *RNA* 2023; 29, 396–401.
5. Wittrup A, Ai A, Liu X, *et al.* Visualizing lipid-formulated siRNA release from endosomes and target gene knockdown. *Nat. Biotechnol.* 2015; 33, 870–876.
6. Gilleron J, Querbes W, Zeigerer A, *et al.* Image-based analysis of lipid nanoparticle–mediated siRNA delivery, intracellular trafficking and endosomal escape. *Nat. Biotechnol.* 2013; 31, 638–646.
7. Maxfield FR, Yamashiro DJ. Endosome Acidification and the Pathways of Receptor-Mediated Endocytosis. In: *Immunobiology of Proteins and Peptides IV*; (Editor: Atassi MZ). 1987; Springer US, 189–198.
8. Huotari J, Helenius A. Endosome maturation: endosome maturation. *EMBO J.* 2011, 30, 3481–3500.
9. Rennick JJ, Johnston APR, Parton RG. Key principles and methods for studying the endocytosis of biological and nanoparticle therapeutics. *Nat. Nanotechnol.* 2021; 16, 266–276.
10. Sahay G, Alakhova DY, Kabanov AV. Endocytosis of nanomedicines. *J. Control. Release* 2010; 145, 182–195.
11. Sahay G, Kim JO, Kabanov AV, Bronich TK. The exploitation of differential endocytic pathways in normal and tumor cells in the selective targeting of nanoparticulate chemotherapeutic agents. *Biomaterials* 2010; 31, 923–933.
12. Schnitzer JE. Gp60 is an albumin-binding glycoprotein expressed by continuous endothelium involved in albumin transcytosis. *Am. J. Physiol.-Heart Circ. Physiol.* 1992; 262, H246–H254.
13. Parton RG, Howes MT. Revisiting caveolin trafficking: the end of the caveosome. *J. Cell Biol.* 2010; 191, 439–441.
14. Qiu, C, Xia, F, Zhang, J, *et al.* Advanced strategies for overcoming endosomal/lysosomal barrier in nanodrug delivery. *Research* 2023; 6, 0148.
15. Huang WC, Burnouf PA, Su YC, *et al.* Engineering chimeric receptors to investigate the size- and rigidity-dependent interaction of PEGylated nanoparticles with cells. *ACS Nano* 2016; 10, 648–662.
16. Bareford L, Swaan P. Endocytic mechanisms for targeted drug delivery. *Adv. Drug Deliv. Rev.* 2007; 59, 748–758.
17. Dautry-Varsat A, Ciechanover A, Lodish HF. pH and the recycling of transferrin during receptor-mediated endocytosis. *Proc. Natl. Acad. Sci.* 1983; 80, 2258–2262.
18. Pelkmans L, Helenius A. Endocytosis via caveolae. *Traffic* 2002, 3, 311–320.
19. Gabrielson NP, Pack DW. Efficient polyethylenimine-mediated gene delivery proceeds via a caveolar pathway in HeLa cells. *J. Control. Release* 2009; 136, 54–61.
20. Lu JJ, Langer R, Chen J. A novel mechanism is involved in cationic lipid-mediated functional siRNA delivery. *Mol. Pharm.* 2009; 6, 763–771.
21. Ghosh A, Sharma M, Zhao Y. Cell-Penetrating protein-recognizing polymeric nanoparticles through dynamic covalent chemistry and double imprinting. *Nat. Commun.* 2024; 15, 3731.
22. Panja P, Jana NR. Arginine-terminated nanoparticles of <10 Nm size for direct membrane penetration and protein delivery for straight access to cytosol and nucleus. *J. Phys. Chem. Lett.* 2020; 11, 2363–2368.

23. Qiu J, Gong S, Alp Y, Medeiros J, Agnello E, Thayumanavan S. Membrane fusion drives facile uptake of cell membrane-coated nanocarriers. *ACS Nano* 2025; 19, 23001–23010.

24. Xu E, Saltzman WM, Piotrowski-Daspit AS. Escaping the endosome: assessing cellular trafficking mechanisms of non-viral vehicles. *J. Control. Release* 2021; 335, 465–480.

25. Du Rietz H, Hedlund H, Wilhelmson, S.; Nordenfelt P, Wittrup A. Imaging small molecule-induced endosomal escape of siRNA. *Nat. Commun.* 2020; 11, 1809.

26. Teo SLY, Rennick JJ, Yuen D, Al-Wassiti H, Johnston APR, Pouton CW. Unravelling cytosolic delivery of cell penetrating peptides with a quantitative endosomal escape assay. *Nat. Commun.* 2021; 12, 3721.

27. Cabral H, Miyata K, Osada K, Kataoka K. Block copolymer micelles in nanomedicine applications. *Chem. Rev.* 2018, 118, 6844–6892.

28. Uchida S, Kinoh H, Ishii T, *et al.* Systemic delivery of messenger RNA for the treatment of pancreatic cancer using polyplex nanomicelles with a cholesterol moiety. *Biomaterials* 2016; 82, 221–228.

29. Chen Z, Lv Z, Sun Y, Chi Z, Qing G. Recent advancements in polyethyleneimine-based materials and their biomedical, biotechnology, and biomaterial applications. *J. Mater. Chem. B* 2020; 8, 2951–2973.

30. Eweje F, Ibrahim V, Shajii A, *et al.* Self-assembling protein nanoparticles for cytosolic delivery of nucleic acids and proteins. *Nat. Biotechnol.* 2025; published online May 15. https://doi.org/10.1038/s41587-025-02664-2.

31. Hubbel J, Hossainy S, Kang S, *et al.* Thermoreversibly assembled polymersomes for highly efficient loading, processing, and delivery of protein and siRNA biologics. *Res Sq.* 2024; preprint.

32. Freeman EC, Weiland LM, Meng WS. Modeling the proton sponge hypothesis: examining proton sponge effectiveness for enhancing intracellular gene delivery through multiscale modeling. *J. Biomater. Sci. Polym. Ed.* 2013; 24, 398–416.

33. Benjaminsen RV, Mattebjerg MA, Henriksen JR, Moghimi SM, Andresen TL. The possible 'proton sponge' effect of polyethylenimine (PEI) does not include change in lysosomal pH. *Mol. Ther.* 2013; 21, 149–157.

34. Godbey WT, Wu KK, Mikos AG. Poly(ethylenimine) and its role in gene delivery. *J. Control. Release* 1999; 60, 149–160.

35. Godbey WT, Wu KK, Mikos AG. Poly(ethylenimine)-mediated gene delivery affects endothelial cell function and viability. *Biomaterials* 2001; 22, 471–480.

36. Lv H, Zhang S, Wang B, Cui S, Yan J. Toxicity of cationic lipids and cationic polymers in gene delivery. *J. Control. Release* 2006; 114, 100–109.

37. Kargaard A, Sluijter JPG, Klumperman B. Polymeric siRNA gene delivery—transfection efficiency versus cytotoxicity. *J. Control. Release* 2019; 316, 263–291.

38. Forrest ML, Koerber JT, Pack DWA. Degradable polyethylenimine derivative with low toxicity for highly efficient gene delivery. *Bioconjug. Chem.* 2003; 14, 934–940.

39. Lin C, Engbersen JF. The role of the disulfide group in disulfide-based polymeric gene carriers. *Expert Opin. Drug Deliv.* 2009; 6, 421–439.

40. Peng, Q, Zhong, Z, Zhuo, R. Disulfide cross-linked polyethylenimines (PEI) prepared via thiolation of low molecular weight PEI as highly efficient gene vectors. *Bioconjug. Chem.* 2008; 19, 499–506.

41. Werfel TA, Jackson MA, Kavanaugh TE, *et al.* Combinatorial optimization of PEG architecture and hydrophobic content improves ternary siRNA polyplex stability, pharmacokinetics, and potency *in vivo*. *J. Control. Release* 2017; 255, 12–26.

42. Hall A, Lächelt U, Bartek J, Wagner E, Moghimi SM. Polyplex evolution: understanding biology, optimizing performance. *Mol. Ther*. 2017; 25, 1476–1490.

43. Zhou Z, Li C, Zhang M, Zhang Q, Qian C, Oupicky D, Sun M. Charge and assembly reversible micelles fueled by intracellular ATP for improved siRNA transfection. *ACS Appl. Mater. Interfaces* 2018; 10, 32026–32037.

44. Lynn DM, Langer R. Degradable poly(β-amino esters): synthesis, characterization, and self-assembly with plasmid DNA. *J. Am. Chem. Soc.* 2000; 122, 10761–10768.

45. Anderson DG, Lynn DM, Langer R. Semi-automated synthesis and screening of a large library of degradable cationic polymers for gene delivery. *Angew. Chem. Int. Ed.* 2003; 42, 3153–3158.

46. Eltoukhy AA, Chen D, Alabi CA, Langer R, Anderson DG. Degradable terpolymers with alkyl side chains demonstrate enhanced gene delivery potency and nanoparticle stability. *Adv. Mater.* 2013; 25, 1487–1493.

47. Routkevitch D, Sudhakar D, Conge M, *et al.* Efficiency of cytosolic delivery with poly(β-amino ester) nanoparticles is dependent on the effective pK_a of the polymer. *ACS Biomater. Sci. Eng.* 2020; 6, 3411–3421.

48. Kim J, Mondal SK, Tzeng SY, *et al.* Poly(ethylene glycol)–poly(beta-amino ester)-based nanoparticles for suicide gene therapy enhance brain penetration and extend survival in a preclinical human glioblastoma orthotopic xenograft model. *ACS Biomater. Sci. Eng.* 2020; 6, 2943–2955.

49. Su X, Fricke J, Kavanagh DG, Irvine DJ. *In vitro* and *in vivo* mRNA delivery using lipid-enveloped pH-responsive polymer nanoparticles. *Mol. Pharm.* 2011; 8, 774–787.

50. Yong H, Lin L, Li Z, *et al.* Tailoring highly branched poly(β-amino ester)s for efficient and organ-selective mRNA delivery. *Nano Lett.* 2024; 24, 9368–9376.

51. Thomas M, Klibanov AM. Enhancing polyethylenimine's delivery of plasmid DNA into mammalian cells. *Proc. Natl. Acad. Sci.* 2002; 99, 14640–14645.

52. Zhou J, Liu J, Cheng CJ, *et al.* Biodegradable poly(amine-co-ester) terpolymers for targeted gene delivery. *Nat. Mater.* 2012; 11, 82–90.

53. Kauffman AC, Piotrowski-Daspit AS, Nakazawa KH, Jiang Y, Datye A, Saltzman WM. Tunability of biodegradable poly(amine-*co*-ester) polymers for customized nucleic acid delivery and other biomedical applications. *Biomacromolecules* 2018; 19, 3861–3873.

54. Suberi A, Grun MK, Mao T, *et al.* Polymer nanoparticles deliver mRNA to the lung for mucosal vaccination. *Sci. Transl. Med.* 2023; 15, eabq0603.

55. Maxfield FR. Weak bases and ionophores rapidly and reversibly raise the pH of endocytic vesicles in cultured mouse fibroblasts. *J. Cell Biol.* 1982; 95, 676–681.

56. Dowdy SF. Overcoming cellular barriers for RNA therapeutics. *Nat. Biotechnol.* 2017; 35, 222–229.

57. Sun JH, Ye C, Bai EH, *et al.* Co-delivery nanoparticles of doxorubicin and chloroquine for improving the anti-cancer effect *in vitro*. *Nanotechnology* 2019; 30, 085101.

58. Xie Y, Yu F, Tang W, *et al.* Synthesis and evaluation of chloroquine-containing DMAEMA copolymers as efficient anti-miRNA delivery vectors with improved endosomal escape and antimigratory activity in cancer cells. *Macromol. Biosci.* 2018; 18, 1.

59. Liu Z, Wu J, Wang N, *et al.* Structure-guided design of endosomolytic chloroquine-like lipid nanoparticles for mRNA delivery and genome editing. *Nat. Commun.* 2025; 16, 4241.

60. Ma Y, Fenton OS. Tannic acid lipid nanoparticles can deliver messenger RNA payloads and improve their endosomal escape. *Adv. Ther.* 2023; 6, 6.

61. Yang MM, Yarragudi SB, Jamieson SMF, Tang M, Wilson WR, Wu Z. calcium enabled remote loading of a weak acid into pH-sensitive liposomes and augmented cytosolic delivery to cancer cells via the proton sponge effect. *Pharm. Res.* 2022; 39, 1181–1195.

62. Wang Y, Xie Y, Kilchrist KV, Li J, Duvall CL, Oupický D. Endosomolytic and tumor-penetrating mesoporous silica nanoparticles for siRNA/miRNA combination cancer therapy. ACS *Appl. Mater. Interfaces* 2020; 12, 4308–4322.

63. Wang L, Ariyarathna Y, Ming X, *et al.* A novel family of small molecules that enhance the intracellular delivery and pharmacological effectiveness of antisense and splice switching oligonucleotides. *ACS Chem. Biol.* 2017; 12, 1999–2007.

64. Bost JP, Ojansivu M, Munson MJ, *et al.* Novel endosomolytic compounds enable highly potent delivery of antisense oligonucleotides. *Commun. Biol.* 2022; 5, 185.

65. Vermeulen LMP, De Smedt SC, Remaut K, Braeckmans K. The proton sponge hypothesis: fable or fact? *Eur. J. Pharm. Biopharm.* 2018; 129, 184–190.

66. Sonawane ND, Szoka FC, Verkman AS. Chloride accumulation and swelling in endosomes enhances DNA transfer by polyamine-DNA polyplexes. *J. Biol. Chem.* 2003; 278, 44826–44831.

67. Lomas H, Massignani M, Abdullah KA, *et al.* Non-cytotoxic polymer vesicles for rapid and efficient intracellular delivery. *Faraday Discuss.* 2008; 139, 143.

68. Nelson CE, Kintzing JR, Hanna A, Shannon JM, Gupta MK, Duvall CL. Balancing cationic and hydrophobic content of PEGylated siRNA polyplexes enhances endosome escape, stability, blood circulation time, and bioactivity *in vivo*. *ACS Nano* 2013; 7, 8870–8880.

69. Manganiello MJ, Cheng C, Convertine AJ, Bryers JD, Stayton PS. Diblock copolymers with tunable pH transitions for gene delivery. *Biomaterials* 2012; 33, 2301–2309.

70. Baljon JJ, Kwiatkowski AJ, Pagendarm HM, *et al*. A cancer nanovaccine for co-delivery of peptide neoantigens and optimized combinations of STING and TLR4 agonists. *ACS Nano* 2024; 18, 6845–6862.

71. Hu Y, Litwin T, Nagaraja AR, *et al.* Delivery of membrane-impermeable molecules in dendritic cells using pH-responsive core–shell nanoparticles. *Nano Lett.* 2007; 7, 3056–3064.

72. Kermaniyan SS, Chen M, Zhang C, *et al.* Understanding the biological interactions of pH-swellable nanoparticles. *Macromol. Biosci.* 2022; 22, 2100445.

73. Yang J, Bahreman A, Daudey G, Bussmann J, Olsthoorn RCL, Kros A. Drug delivery via cell membrane fusion using lipopeptide modified liposomes. *ACS Cent. Sci.* 2016; 2, 621–630.

74. Koitabashi K, Nagumo H, Nakao M, *et al.* Acidic pH-induced changes in lipid nanoparticle membrane packing. *Biochim. Biophys. Acta Biomembr.* 2021; 1863, 183627.

75. Ong ZY, Yang C, Cheng W, *et al.* Biodegradable cationic poly(carbonates): effect of varying side chain hydrophobicity on key aspects of gene transfection. *Acta Biomater.* 2017; 54, 201–211.

76. Convertine AJ, Diab C, Prieve M, *et al.* pH-responsive polymeric micelle carriers for siRNA drugs. *Biomacromolecules* 2010; 11, 2904–2911.

77. Kongkatigumjorn N, Smith SA, Chen M, *et al.* Endosomal escape using pH-responsive nanoparticles with tunable disassembly. *ACS Appl. Nano Mater.* 2018; 1, 3164–3173.

78. Luo M, Wang H, Wang Z, *et al.* A STING-activating nanovaccine for cancer immunotherapy. *Nat. Nanotechnol.* 2017; 12, 648–654.

79. Putnam D, Gentry CA, Pack DW, Langer R. Polymer-based gene delivery with low cytotoxicity by a unique balance of side-chain termini. *Proc. Natl. Acad. Sci.* 2001; 98, 1200–1205.

80. Midoux, P, Monsigny, M. Efficient gene transfer by histidylated polylysine/pDNA complexes. *Bioconjug. Chem.* 1999; 10, 406–411.

81. Lu D, An Y, Feng S, *et al.* Imidazole-bearing polymeric micelles for enhanced cellular uptake, rapid endosomal escape, and on-demand cargo release. *AAPS PharmSciTech* 2018; 19, 2610–2619.

82. Wu H, Zhu L, Torchilin VP. pH-sensitive poly(histidine)-PEG/DSPE-PEG co-polymer micelles for cytosolic drug delivery. *Biomaterials* 2013; 34, 1213–1222.

83. Jobdeedamrong A, Crespy D. Redox-responsive polyprodrugs: recent innovations in reduction- and oxidation-responsive drug delivery systems. *Chem. Mater.* 2025; 37, 2073–2086.

84. Kanjilal P, Dutta K, Thayumanavan S. Thiol-disulfide exchange as a route for endosomal escape of polymeric nanoparticles. *Angew. Chem. Int. Ed.* 2022; 61, e202209227.

85. Mo Y, Cheng MHY, D'Elia A, *et al.* Light-activated siRNA endosomal release (LASER) by porphyrin lipid nanoparticles. *ACS Nano* 2023; 17, 4688–4703.

86. Yuan Y, Zhang C, Liu B. A photoactivatable AIE polymer for light-controlled gene delivery: concurrent endo/lysosomal escape and DNA unpacking. *Angew. Chem. Int. Ed.* 2015; 54, 11419–11423.

87. Selby LI, Cortez-Jugo CM, Such GK, Johnston APR. Nanoescapology: progress toward understanding the endosomal escape of polymeric nanoparticles. *WIREs Nanomed. Nanobiotechnol*. 2017; 9, e1452.

88. Romani B, Engelbrecht S, Glashoff RH. Functions of Tat: the versatile protein of human immunodeficiency virus type 1. *J. Gen. Virol.* 2010; 91, 1–12.

89. Vivès E, Brodin P, Lebleu B. A truncated HIV-1 tat protein basic domain rapidly translocates through the plasma membrane and accumulates in the cell nucleus. *J. Biol. Chem.* 1997; 272, 16010–16017.

90. Hameed DS, Sapmaz A, Gjonaj L, Merkx R, Ovaa H. enhanced delivery of synthetic labelled ubiquitin into live cells by using next-generation Ub–TAT conjugates. *ChemBioChem* 2018; 19, 2553–2557.

91. Lee YJ, Datta S, Pellois JP. Real-time fluorescence detection of protein transduction into live cells. *J. Am. Chem. Soc.* 2008; 130, 2398–2399.

92. Jones AT, Sayers EJ. Cell entry of cell penetrating peptides: tales of tails wagging dogs. *J. Control. Release* 2012; 161, 582–591.

93. Mitchell D J, Steinman L, Kim DT, Fathman CG, Rothbard JB. Polyarginine enters cells more efficiently than other polycationic homopolymers. *J. Pept. Res.* 2000; 56, 318–325.

94. Wharton SA, Martin SR, Ruigrok RWH, Skehel JJ, Wiley DC. Membrane fusion by peptide analogues of influenza virus haemagglutinin. *J. Gen. Virol.* 1988; 69, 1847–1857.

95. Deshayes S, Heitz A, Morris MC, Charnet P, Divita G, Heitz F. Insight into the mechanism of internalization of the cell-penetrating carrier peptide Pep-1 through conformational analysis. *Biochemistry* 2004; 43, 1449–1457.

96. Cleal K, He LD, Watson PT, Jones A. Endocytosis, intracellular traffic and fate of cell penetrating peptide based conjugates and nanoparticles. *Curr. Pharm. Des.* 2013; 19, 2878–2894.

97. Nischan N, Herce HD, Natale F, *et al.* Covalent attachment of cyclic TAT peptides to GFP results in protein delivery into live cells with immediate bioavailability. *Angew. Chem. Int. Ed.* 2015; 54, 1950–1953.

98. Lättig-Tünnemann G, Prinz M, Hoffmann D, *et al.* Backbone rigidity and static presentation of guanidinium groups increases cellular uptake of arginine-rich cell-penetrating peptides. *Nat. Commun.* 2011; 2, 453.

99. Ruseska I, Zimmer A. Internalization mechanisms of cell-penetrating peptides. *Beilstein J. Nanotechnol.* 2020; 11, 101–123.

100. Tünnemann G, Martin RM, Haupt S, Patsch C, Edenhofer F, Cardoso MC. Cargo-dependent mode of uptake and bioavailability of TAT-containing proteins and peptides in living cells. *FASEB J.* 2006, 20, 1775–1784.

101. Tian Y, Zhou M, Shi H, *et al.* Integration of cell-penetrating peptides with rod-like bionanoparticles: virus-inspired gene-silencing technology. *Nano Lett.* 2018; 18, 5453–5460.

102. Liang JF, Yang VC. Insulin-cell penetrating peptide hybrids with improved intestinal absorption efficiency. *Biochem. Biophys. Res. Commun.* 2005; 335, 734–738.

103. Regen SL. Membrane-disrupting molecules as therapeutic agents: a cautionary note. *JACS Au* 2021; 1, 3–7.

104. Moschos SA, Jones SW, Perry MM, *et al.* Lung delivery studies using siRNA conjugated to TAT(48–60) and penetratin reveal peptide induced reduction in gene expression and induction of innate immunity. *Bioconjug. Chem.* 2007; 18, 1450–1459.

105. Xie J, Bi Y, Zhang H, *et al.* Cell-penetrating peptides in diagnosis and treatment of human diseases: from preclinical research to clinical application. *Front. Pharmacol.* 2020; 11, 697

106. Zhao Y, Jiang H, Yu J, Wang L, Du J. Engineered histidine-rich peptides enhance endosomal escape for antibody-targeted intracellular delivery of functional proteins. *Angew. Chem. Int. Ed.* 2023; 62, e202304692.

107. Akishiba M, Takeuchi T, Kawaguchi Y, *et al.* Cytosolic antibody delivery by lipid-sensitive endosomolytic peptide. *Nat. Chem.* 2017; 9, 751–761.

108. Narum S, Deal B, Ogasawara H, Mancuso JN, Zhang J, Salaita K. An endosomal escape trojan horse platform to improve cytosolic delivery of nucleic acids. *ACS Nano* 2024; 18, 6186–6201.

109. Szabó I, Yousef M, Soltész D, Bató C, Mező G, Bánóczi Z. Redesigning of cell-penetrating peptides to improve their efficacy as a drug delivery system. *Pharmaceutics* 2022; 14, 907.

110. Nielsen EJB, Yoshida S, Kamei N, *et al.* *In vivo* proof of concept of oral insulin delivery based on a co-administration strategy with the cell-penetrating peptide penetratin. *J. Control. Release* 2014; 189, 19–24.

111. Najjar K, Erazo-Oliveras A, Brock DJ, Wang TY, Pellois JP. An L- to d-amino acid conversion in an endosomolytic analog of the cell-penetrating peptide tat influences proteolytic stability, endocytic uptake, and endosomal escape. *J. Biol. Chem.* 2017; 292, 847–861.

112. Veiman, K.-L, Künnapuu, K, Lehto, T, *et al.* PEG Shielded MMP sensitive CPPs for efficient and tumor specific gene delivery *in vivo. J. Control. Release* 2015; 209, 238–247.

113. Hong L, Wang Z, Wei X, Shi J, Li C. Antibodies against polyethylene glycol in human blood: a literature review. *J. Pharmacol. Toxicol. Methods* 2020; 102, 106678.

114. Cai H, Liang Z, Huang W, Wen L, Chen G. Engineering PLGA nano-based systems through understanding the influence of nanoparticle properties and cell-penetrating peptides for cochlear drug delivery. *Int. J. Pharm.* 2017; 532, 55–65.

115. Ma P, Yu H, Zhang X, *et al.* Increased active tumor targeting by an Avβ3-targeting and cell-penetrating bifunctional peptide-mediated dendrimer-based conjugate. *Pharm. Res.* 2017; 34, 121–135.

116. Perillo, E, Allard-Vannier, E, Falanga, A, *et al.* Quantitative and qualitative effect of gH625 on the nanoliposome-mediated delivery of mitoxantrone anticancer drug to HeLa cells. *Int. J. Pharm.* 2015; 488, 59–66.

117. Song K, Nguyen DC, Luu T, *et al.* A mannosylated polymer with endosomal release properties for peptide antigen delivery. *J. Control. Release* 2023; 356, 232–241.

118. Evans BC, Fletcher RB, Kilchrist KV, *et al.* An anionic, endosome-escaping polymer to potentiate intracellular delivery of cationic peptides, biomacromolecules, and nanoparticles. *Nat. Commun.* 2019; 10, 5012.

119. Evans BC, Hocking KM, Kilchrist KV, Wise ES, Brophy CM, Duvall CL. Endosomolytic nano-polyplex platform technology for cytosolic peptide delivery to inhibit pathological vasoconstriction. *ACS Nano* 2015; 9, 5893–5907.

120. Tripathi PP, Arami H, Banga I, Gupta J, Gandhi S. Cell penetrating peptides in preclinical and clinical cancer diagnosis and therapy. *Oncotarget* 2018; 9, 37252–37267.

121. Garcea RL, Meinerz NM, Dong M Funke H, Ghazvini S, Randolph TW. Single-administration, thermostable human papillomavirus vaccines prepared with atomic layer deposition technology. *NPJ Vaccines* 2020; 5, 45.

122. Beach MA, Nayanathara U, Gao Y, *et al.* Polymeric nanoparticles for drug delivery. *Chem. Rev.* 2024; 124, 5505–5616.

AFFILIATIONS

Yvonne Yoyo Ma, **Parul Sirohi**, and **Ashutosh Chilkoti**, Pratt School of Engineering, Duke University, Durham NC, USA

AUTHORSHIP & CONFLICT OF INTEREST

Contributions: The named authors take responsibility for the integrity of the work as a whole, and have given their approval for this version to be published.

Acknowledgements: None.

Disclosure and potential conflicts of interest: The authors have no conflicts of interest.

Funding declaration: The authors received no financial support for the research, authorship and/or publication of this article.

ARTICLE & COPYRIGHT INFORMATION

Article source: Invited; externally peer reviewed.

Submitted for peer review: Jul 28, 2025.

Revised manuscript received: Sep 25, 2025.

Publication date: Oct 16, 2025.

BIOCONJUGATION INSIGHTS

DRIVING IMPROVEMENTS IN DELIVERY AND STABILITY

SPOTLIGHT

INNOVATOR INSIGHT

Design and production of antibody PEG-conjugates for extended ocular retention

Stacy L Capehart, Joshua D Slocum, Tobin E Brown, Alexander D Jackson, Samantha R Summers, Peter CS Woodham, Alexei Kazantsev, Marion Weir, Sangyuel Han, and Eric S Furfine

Herein, we report the site-specific conjugation of polyethylene glycol polymers to increase the vitreal half-life of two antibodies that target a transmembrane receptor protein found in the eye. The resulting conjugates' design, optimization, purification, and characterization are described. Surface plasmon resonance (SPR) analysis demonstrated that the PEG-conjugated antibodies retained binding affinity to the target proteins, compared to the parental unconjugated antibody. The PEG-conjugated antibodies exhibited a slower rate of vitreal clearance compared to the unmodified antibodies in a New Zealand white rabbit ocular pharmacokinetic study.

Bioconjugation Insights 2025; 1(4), 143–156 · DOI: 10.18609/bci.2025.026

Protein therapeutics developed for treating ocular diseases require dosing as frequently as once per month due to their short vitreal half-lives [1]. A slower rate of vitreal clearance can reduce dosing frequency, likely improving patient compliance and positively affecting treatment outcomes [2]. Increasing the apparent hydrodynamic radius of protein therapeutics has been shown to slow the rate of vitreal clearance [3]. Modifying antibodies, their fragments or mimetics with polymers, such as polyethylene glycol (PEG) [3–7], or phosphorylcholine biopolymers [8] increases the hydrodynamic radius and thus the vitreal half-lives. To attach a polymer of interest to an antibody therapeutic, the conjugation strategy should be site-specific, proceed with high conversion, and minimally affect antibody function [9,10].

Herein, the design and chemical conjugation of PEG polymers to an antibody and an antibody-receptor fusion that target a transmembrane receptor protein are described. The resulting conjugates are assessed for purity, *in vitro* binding, and *in vivo* ocular retention in a New Zealand white rabbit pharmacokinetic study.

MATERIALS & METHODS

Materials

Cysteamine hydrochloride and Tris (2-carboxyethyl) phosphine hydrochloride (TCEP-HCl) were purchased from Sigma-Aldrich (St Louis, MO, USA). Methoxy-PEG-(CH2)3NHCO(CH2)2-MAL MW 5,000 (α-[3-(3-Maleimido-1-oxopropyl)amino] propyl-ω-methoxy, polyoxyethylene), Methoxy-PEG-(CH2)3NHCO(CH2)2-MAL, MW 20,000 (α-[3-(3-Maleimido-1-oxopropyl)amino]propyl-ω-methoxy, polyoxyethylene), and 2 arm branched PEG,-(CH2)3NHCO(CH2)2-MAL, MW 40,000 (2,3-Bis(methylpolyoxyethyleneoxy)-1-{[3-(3-maleimido-1-oxopropyl) amino]propyloxy} propane) were obtained from NOF America Corporation (White Plains, NY). According to the manufacturer, the Polydispersity Index (PDI) for all polymers was ~1.1. Endotoxin levels were measured using the Endosafe® Nexgen-PTS instrument using 0.5–0.005 EU/mL CRL test cartridges sourced from Charles River Laboratories (Wilmington, MA, USA).

Protein expression, bioconjugation, and purification

Antibodies were expressed using the ThermoFisher Scientific (Waltham, MA) Expi293™ transient expression system according to the manufacturer's protocols. Clarified cell culture supernatant was purified with a HiTrap MabSelect PrismA™ column (Cytiva, Marlborough, MA), equilibrating with 20 mM sodium phosphate, 150 mM NaCl, pH 7.2. Antibodies captured on the column were eluted with 100 mM sodium citrate, pH 3.5, and neutralized with 1M Tris, pH 8.0 (Teknova, Hollister, CA, USA).

Following purification, antibodies were exchanged into 50 mM sodium phosphate, 150 mM NaCl, 2.5 mM EDTA, pH 7.2. Antibodies at 20 μM were reduced with either cysteamine-HCl (50 mM) for 1 h or TCEP-HCl (1 mM) for 15 min at room temperature. Following reduction, excess reducing agent was removed using a HiTrap™ Desalting column (Cytiva) equilibrated with 50mM sodium phosphate, 15 mM NaCl, 2.5 mM EDTA, pH 7.2. Following desalting, a 10-fold molar excess of either 5 kDa PEG, 20 kDa PEG, or 40 kDa PEG was added to the reduced material, and the reaction proceeded at room temperature for 1.5 h. PEGylated material was then captured on a HiTrap SP High Performance column (Cytiva) equilibrated with 20 mM sodium acetate, pH 4.6, and eluted over a linear gradient with 20 mM sodium acetate, 1 M NaCl, pH 4.6.

Characterization

SDS-PAGE

NuPAGE™ 3–8% tris-acetate or NuPAGE 4–12% bis-tris gels (ThermoFisher Scientific) were used for SDS-PAGE analysis. Color-coded pre-stained protein marker 10–250 kDa from Cell Signaling Technology (Danvers, MA, USA) was used as a molecular weight marker. Non-reduced protein samples (5 μg) were combined with 4x lithium dodecyl sulfate (LDS), and the samples were run without heating. Reduced protein samples (5 μg) were combined with dithiothreitol (5 mM) in 4× LDS and heated for 5 minutes at 95 °C. Gels were stained with SimplyBlue™ SafeStain (ThermoFisher Scientific) according to the manufacturer's instructions.

HPLC

High-pressure liquid chromatography (HPLC) was performed on an Agilent (Santa Clara, CA, USA) 1100 Series HPLC at room temperature. Sample analysis for all HPLC experiments was achieved with an inline diode array detector (DAD) and monitoring absorbance at 280 nm (A280). Chromatograms were analyzed using the Agilent ChemStation software.

For Size Exclusion High Pressure Liquid Chromatography (SEC-HPLC), protein samples (10 µg) were injected into a Sepax Technologies (Newark, DE) Zenix SEC-300, 3 µm, 300 Å, 7.8 x 300 mm column flowing at 0.5 mL/min for 40 min. The mobile phase was 1X PBS, 100 mM arginine, 0.5 mM EDTA, pH 6.7. A Bio-Rad (Hercules, CA, USA) gel filtration standard was used to relate the retention time to the expected molecular weight. For Reversed Phase Liquid Chromatography (RP-HPLC), protein samples (10 µg) were injected onto an Agilent AdvanceBio RP-mAb Diphenyl, 4.6 × 150 mm, 3.5 µm, flowing at 0.5 mL/min. The mobile phase was a linear gradient of 0.1% trifluoroacetic acid (TFA) in HPLC-grade water and 0.1% TFA in HPLC-grade acetonitrile sourced from ThermoFisher Scientific (Waltham, MA, USA).

SPR

Surface plasmon resonance (SPR) experiments were performed on a Biacore3000 instrument using CM5 sensor chips (Cytiva) at 25 °C. Antigen immobilization was carried out using *N*-hydroxysuccinimide (NHS)/1-Ethyl-3-[3-dimethylaminopropyl]carbodiimide (EDC) coupling. A 100 nM, 33.3 nM, 11.1 nM, 3.7 nM, and 1.2 nM solution of each antibody was injected at 30 µL/min for 300 s over a surface containing immobilized antigen, and dissociation was monitored for 900 s. The combined kinetic traces were fit to a 1:1 interaction model using Scrubber software (BioLogic Software, Canberra, Australia), and the equilibrium dissociation constant (K_D) and standard deviation are based on the combined fit in a single experiment.

Ocular pharmacokinetic (PK) study

Formulation

EYLEA® was purchased from Myonex (Horsham, PA) and diluted into the EYLEA formulation buffer (10 mM sodium phosphate, 40 mM NaCl, 0.03% polysorbate-20, 5% sucrose) such that the final aflibercept concentration was 2 mg/mL. All other test articles were formulated in 1X PBST (phosphate-buffered saline containing 0.01% polysorbate-20) at 2 mg/mL and 10 mg/mL for the PRO085 and PRO504 ocular PK studies, respectively. All test articles were filtered through a 0.22 µm Steriflip filter (Millipore, Burlington, MA, USA), and endotoxin was measured below 0.1 EU/mg.

Study design

For the PK study on PRO085 and PEGylated variants, 100 µg intravitreal injections were administered to male New Zealand White rabbits. For each cohort, six animals were dosed on day zero. On days 1, 3, and 7, animals were euthanized, and both eyes were harvested and frozen prior to dissection and collection of vitreous humor. The vitreous humor samples were diluted 1:5 in 1X PBST (phosphate-buffered saline with 0.1% polysorbate-20) without homogenization and stored at −70 °C until analysis.

For the PK study on PRO504 and PEGylated variants, 500 µg intravitreal injections were administered to male New Zealand White rabbits. For each cohort, three or four animals were dosed on day 0. On days 1, 3, 7, and 14, animals were euthanized, and both eyes were harvested and frozen prior to dissection and collection of vitreous humor. The vitreous humor samples were diluted 1:5 in 1× PBST (phosphate-buffered saline with 0.1% polysorbate-20) without homogenization and stored at −70 °C until analysis.

Enzyme-linked immunosorbent assay (ELISA)

Total drug levels in the vitreous humor were quantified using two different ELISAs. All incubations were performed with shaking at 420 rpm unless otherwise indicated. High-binding microtiter plates (Greiner Bio One, Monroe, NC, USA) were coated overnight at 4 °C with an anti-human IgG in 100 mM carbonate, pH 9.5, without

agitation. The coated plate was washed with 1× PBST (phosphate-buffered saline with 0.1% polysorbate-20) containing 150 mM sodium chloride and blocked with 5% bovine serum albumin in 1X PBST for 1 h at 37 °C. After washing, test articles and their corresponding controls were incubated for 1.5 h at room temperature.

For PRO085, PRO171 + [2×5 kDa PEG], PRO171 + [2×20 kDa PEG], PRO504, PRO593 + [2×20 kDa PEG], the plates were washed and incubated with biotinylated antigen for 1.5 h at room temperature. The plates were rewashed, incubated with streptavidin conjugated HRP (R&D Systems, Minneapolis, MN) for 1 h at room temperature, and protected from light.

For aflibercept, the plates were washed and then incubated with a polyclonal goat anti-human IgG-HRP conjugate for 1 h at room temperature and protected from light.

The plate was washed a final time, developed with WesternBright chemiluminescent HRP substrate (Advansta Inc., San Jose, CA, USA) according to the manufacturer's protocols, and read in a Molecular Devices SpectraMax® M5 plate reader.

RESULTS & DISCUSSION

Antibodies PRO085 and PRO504, depicted in the illustrations in **Figure 1**, were selected for this study. These antibodies target the extracellular domain of a one-pass transmembrane protein receptor (protein A, target cannot be disclosed), and PRO504 contains a C-terminal fusion that binds to a soluble signaling protein (protein B, target cannot be disclosed). To achieve site-specific cysteine modification with maleimide-functionalized polyethylene glycol (PEG), several variants of the parent antibodies were produced, and the conjugation conditions were optimized for each construct. For each parent antibody, one cysteine conjugation variant was selected to be scaled and evaluated in a rabbit ocular pharmacokinetic study.

FIGURE 1

The target parent antibodies, PRO085 and PRO504.

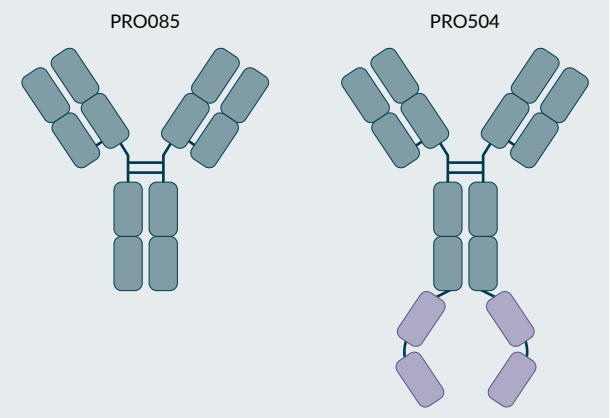

PRO085 construct design

Several N-terminal and C-terminal PRO085 variants were designed and produced, as shown in **Figure 2**. To target the N-terminus of the light chain, an unpaired cysteine residue was directly appended to the parental light chain (PRO086) or included in a five-residue N-terminal linker (DICGS, PRO087, or CDGSG, PRO088). Analogous constructs were made to target the N-terminus of the heavy chain, including an appended cysteine (PRO140) and five-residue linkers (PRO141 and PRO142). To target the C-terminus of the light chain, nine residue extensions comprised of glycine-serine flexible spacers were chosen to flank the unpaired cysteine residue (PRO144). For PRO143, a lysine residue was positioned next to the unpaired cysteine residue to lower the pKa of the reactive cysteine, thus improving its ability to be modified site-selectively **[11]**. A similar approach was selected to target the C-terminus of the heavy chain, as shown in **Figure 2D** for PRO145. Several highly reactive engineered cysteine residues have been described, and we sought to apply this strategy to the conjugation of PEG to PRO085 by introducing the reported V205C (PRO172), S112C (PRO173), A114C

FIGURE 2

Schematics for all PRO085 variants for cysteine PEGylation.

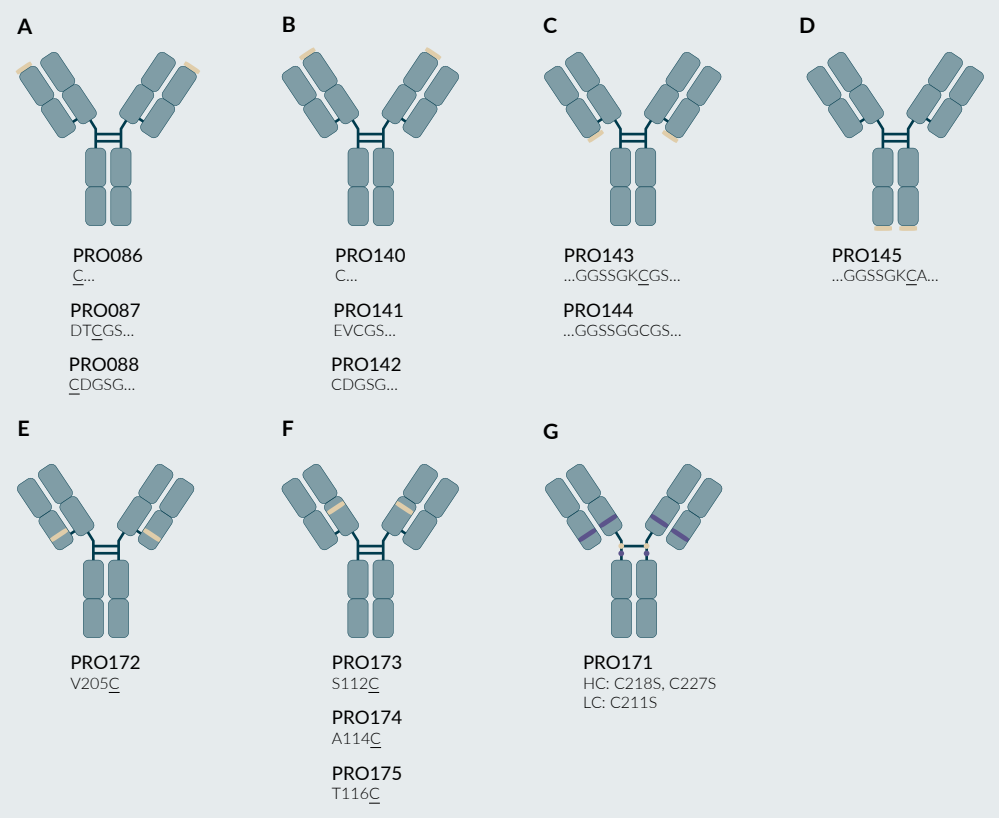

(A) N-terminal light chain variants (PRO086, PRO087, PRO088). (B) N-terminal heavy chain variants (PRO140, PRO141, PRO142). (C) C-terminal light chain variants (PRO143, PRO144). (D) C-terminal heavy chain variants (PRO145). (E) light chain variants (PRO172). (F) heavy chain variants (PRO173, PRO174, PRO175). (G) heavy chain C218S, C227S and light chain C214S to modify the heavy chain C224. Light brown ovals represent targeted cysteine residues (native or mutant), and purple ovals represent residues mutated from cysteine to serine.

(PRO174), and T116C (PRO175) mutations [12]. Finally, we introduced heavy chain C218S, C227S, and light chain C214S point mutations to target the modification of the upper hinge, Cys 224 [13].

PRO085 PEG conjugation

Following reported reduction, re-oxidation, and conjugation procedures, PRO086-PRO088, PRO140-PRO145, and PRO171-PRO175 were evaluated for modification with maleimide-functionalized 5 kDa or 20 kDa linear PEG [12].

N-terminal cysteines were found to be more readily modified than C-terminal cysteines, and cysteines on the heavy chain were more readily modified than those on the light chain ([PRO140, PRO141, PRO142] > [PRO086, PRO087, PRO088] > PRO145 > [PRO143, PRO144]). All antibodies were assessed for binding to their intended target, A and B, using SPR, where the primary objective was to verify the interaction between the PEG-conjugated compounds. Including a mixture of vitreous proteins could introduce non-specific binding, thereby complicating the interpretation of the reported dissociation constants (KDs) for the targets of interest. Antibodies conjugated at N-terminal cysteines showed decreased binding signal via

SPR to Target A relative to those modified at C-terminal cysteines.

Modification occurred more readily on light chain V205C (PRO172) and heavy chain A114C (PRO174) than heavy chain S112C (PRO173) and heavy chain T116C (PRO175).

Upon optimization of reduction and conjugation conditions, PRO171 converted into ~65% of the desired [2 × PEG] conjugated antibody, as determined by SDS-PAGE (schematic shown in **Figure 3**). Due to the high conversion to the desired doubly PEG modified product, PRO171 was selected to

FIGURE 3

Optimized reduction and conjugation strategy for PRO171 to yield PRO171 + [2 × 5 kDa PEG] or PRO171 + [2 × 20 kDa PEG].

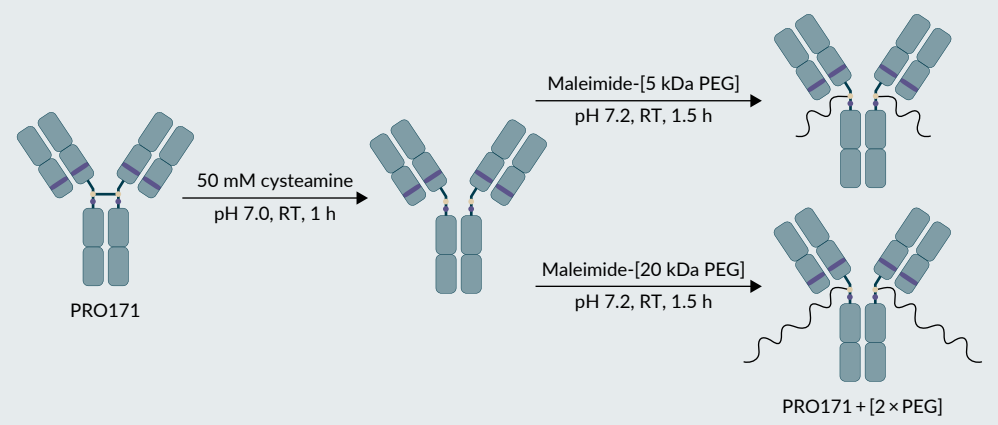

FIGURE 4

Purification of PRO171 + [2 × 5 kDa PEG] and PRO171 + [2 × 20 kDa PEG].

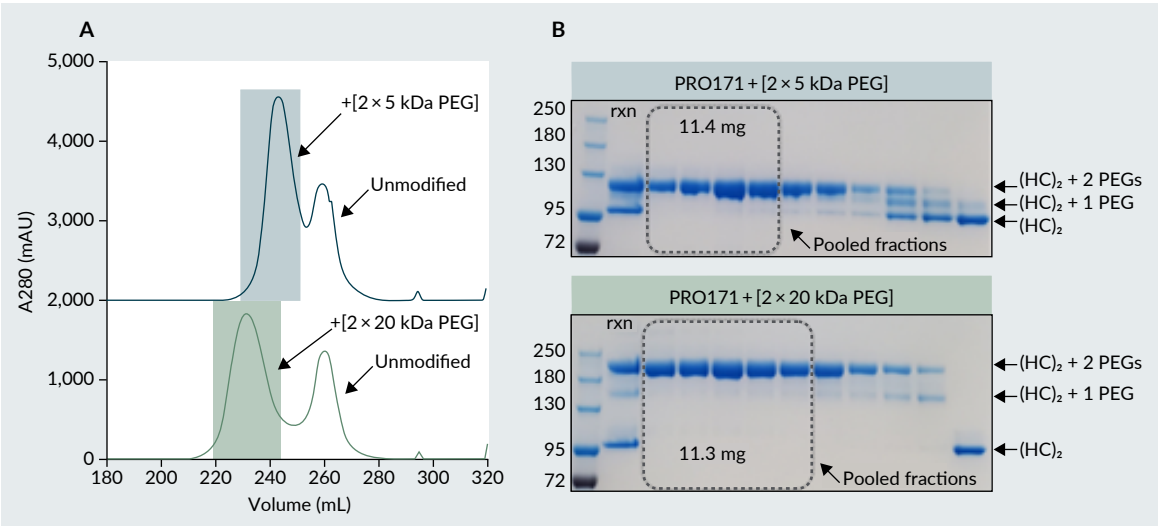

(A) Cation exchange chromatography was used to separate PRO171 + [2 × 5 kDa PEG] and PRO171 + [2 × 20 kDa PEG] from unmodified or singly modified PRO171. Representative fast protein liquid chromatography (FPLC) traces. (B) Reduced SDS-PAGE are shown above for PRO171 + [2 × 5 kDa PEG] and PRO171 + [2 x 20 kDa PEG], highlighted in blue and green, respectively. For the SDS-PAGE, the crude reaction mixture was run in lane 1, and all pooled fractions are outlined in the grey dotted box.

scale and evaluate in a rabbit ocular pharmacokinetic study.

Following the scaled 5 kDa and 20 kDa PEG conjugation of PRO171, the material was purified using a strong cation exchange column on a fast protein liquid chromatography (FPLC) system, and the resulting fractions were assessed for purity by SDS-PAGE, as shown in **Figure 4A and B**. PRO171 + [2 × PEG] eluted early in the gradient, followed by the PRO171 + [1 × PEG], and unmodified PRO171. Fractions corresponding to doubly PEG-modified PRO171 were pooled and analyzed by SDS-PAGE, SEC-HPLC, RP-HPLC, and binding by SPR, as shown in **Figure 5A–D**.

Non-reduced SDS-PAGE analysis revealed PRO085 migrates as a single band at the expected molecular weight. PRO171 + [2 × 5 kDa PEG] and PRO171 + [2 × 20 kDa PEG] have three separate bands when analyzed by SDS-PAGE. PRO171 lacks four disulfide bonds compared to PRO085, which likely influences its migration on SDS-PAGE. The top, middle, and bottom bands are tentatively assigned to the PEG conjugated heavy chain dimer, PEG conjugated heavy chain monomer, and unpaired light chain, respectively.

Analysis by SEC-HPLC measured at >90% main peak. PRO085, PRO171 + [2 × 5 kDa PEG], PRO171 + [2 × 20 kDa PEG] had retention times of 15.6 min, 14.4 min, and 12.3 min, respectively. The retention time for PRO085 is consistent with a typical retention time for antibodies, indicating that the antibody remains intact under native conditions. The comparison of retention times between unmodified and PEG-conjugated material indicates that PRO171 + [2 × 20 kDa PEG] has the largest hydrodynamic radius, followed by PRO171 + [2 × 5 kDa PEG], and finally PRO085, as expected.

By RP-HPLC, purities were >90% main peak. PRO171 + [2 × 20 kDa PEG] was retained the longest, followed by PRO171 + [2 × 5 kDa PEG], and finally PRO085. This retention time increases PEG length, with larger PEG species interacting

FIGURE 5

Characterization of PRO085, PRO171 + [2 × 5 kDa PEG], and PRO171 + [2 × 20 kDa PEG] by (A) SDS-PAGE, (B) SEC-HPLC, (C) RP-HPLC, and (D) SPR.

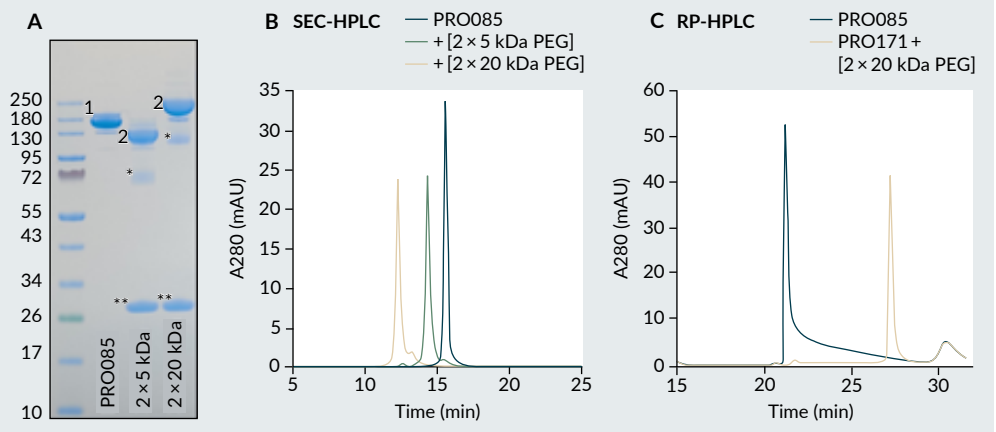

D

Variant	KD (pM) to target protein A
PRO085	477 ± 1
PRO171 + [2 × 5 kDa PEG]	623 ± 1
PRO171 + [2 × 20 kDa PEG]	971 ± 5

more strongly with the stationary phase and being retained longer on the column, as expected.

PRO085, PRO171 + [2 × 5 kDa], and PRO171 + [2 × 20 kDa] PEG bound the soluble extracellular domain of the target receptor with comparable equilibrium binding constants (K_D) of 0.81 nM, 0.76 nM, and 1.22 nM, respectively.

The stability of PEG-conjugated PRO085 was evaluated at 40 °C over 30 days. The primary degradation pathway involved the loss of one PEG moiety from the doubly modified PRO085, which plateaued at approximately 35%. Loss of both PEGs accounted for no more than 8% of the total protein. Despite this degradation, the material was deemed suitable for use in the ocular pharmacokinetic (PK) study described herein. Given the 7-day duration of the PK study, it is likely that the doubly PEG-conjugated species remained as the predominant form throughout the study.

PRO085 Ocular PK Study

Four cohorts of New Zealand White rabbits were dosed with 100 µg of PRO085, PRO171 + [2 × 5 kDa PEG], PRO171 + [2 × 20 kDa PEG], and aflibercept,

FIGURE 6

Total drug measured in vitreous humor by ELISA for (A) aflibercept, (B) PRO085, (C) PRO171 + [2 × 5 kDa PEG], and (D) PRO171 + [2 × 20 kDa PEG].

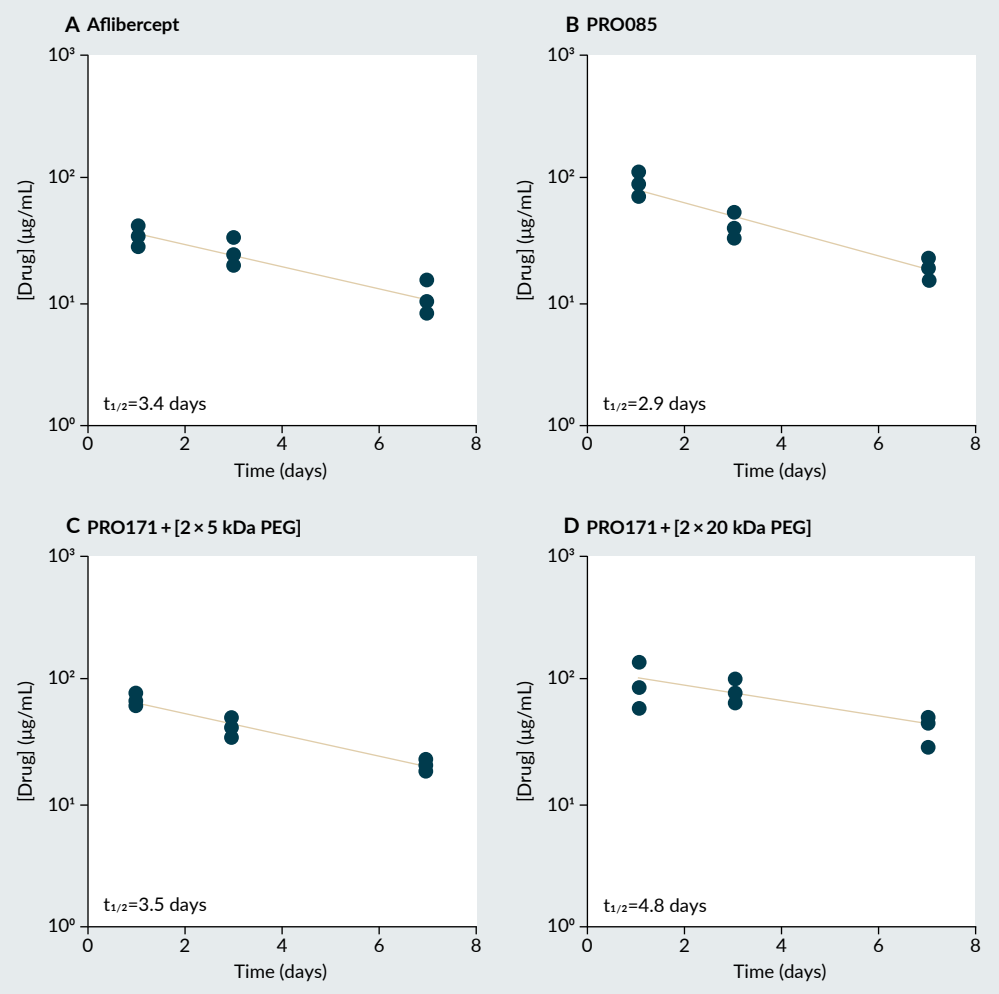

respectively. An ELISA was used to analyze vitreous humor samples collected on days 1, 3, and 7 for total drug, and the half-life was determined for the values fit to a log-linear regression. As shown in **Figure 6A**, the half-life was 3.4 days for aflibercept, similar to the reported value of 3.9 days [14]. PRO171 + [2 × 20 kDa PEG] was retained the longest in the vitreous with a measured half-life of 4.8 days, followed by PRO171 + [2 × 5 kDa PEG] at 3.5 days, and finally unmodified PRO085 at 2.9 days, as shown in **Figure 6B–D**.

PRO504 construct design

Guided by insights from the work with PRO085, a focused set of constructs was designed to enable efficient PEG conjugation **(Figure 7)**. All variants included the light chain C214S mutation that reduces undesired light chain PEG conjugation of the PRO085 variants described above. PRO592 included the heavy chain C227S mutation to target modification of the upper hinge C224, while PRO596 included heavy chain C224S mutation to target modification of the lower hinge, C227. PRO593, PRO594, and PRO595 included mutations of C224S and C227S to remove the heavy chain hinge cysteines, thus preventing undesired PEGylation sites. In addition, unpaired cysteines were introduced on either the C-terminus (PRO593) or directly before (PRO594) or after (PRO595) a linker connecting the C-terminal fusion protein.

Upon optimization of reduction and conjugation conditions, PRO592 and PRO596 converted to 75% and 40% of the desired doubly PEG conjugated product, as assessed by SDS-PAGE. All constructs lacking the hinge disulfide bonds (PRO593, PRO594, PRO595) had near quantitative conversion to the desired doubly PEG conjugated product as assessed by SDS-PAGE. C-terminal variant PRO593 was selected for scaled conjugation and subsequent evaluation in a rabbit ocular pharmacokinetic study due to its high conversion to the desired product and reduced impact of conjugation on stability and target protein binding.

A 40 kDa branched PEG was selected for scaled conjugation to PRO593 to further extend the ocular retention compared to 5 kDa or 20 kDa PEG conjugates **(Figure 8)**. Following the scaled 40 kDa PEG conjugation of PRO593, the material was purified using a strong cation exchange column on

FIGURE 7

All PRO504 variants for cysteine PEGylation.

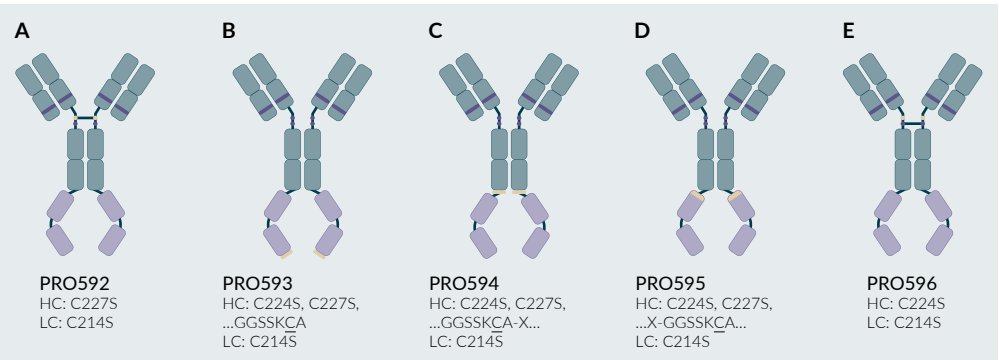

All variants included the light chain C214S mutation as well as heavy chain mutations including: (A) C227S (PRO592); (B) C224S, C227S and a C-terminal extension (PRO593); (C) C224S and C227S with an introduced interior cysteine (PRO594); (D) C224S and C227S with an introduced interior cysteine (PRO595); and (E) C224S (PRO596). Light brown ovals represent targeted cysteine residues (native or mutant), and purple ovals represent residues mutated from cysteine to serine. For PRO594 and PRO595, the 'X' denotes an undisclosed linker.

FIGURE 8

Optimized reduction and conjugation strategy for PRO593 to yield PRO593 + [2 × 40 kDa PEG].

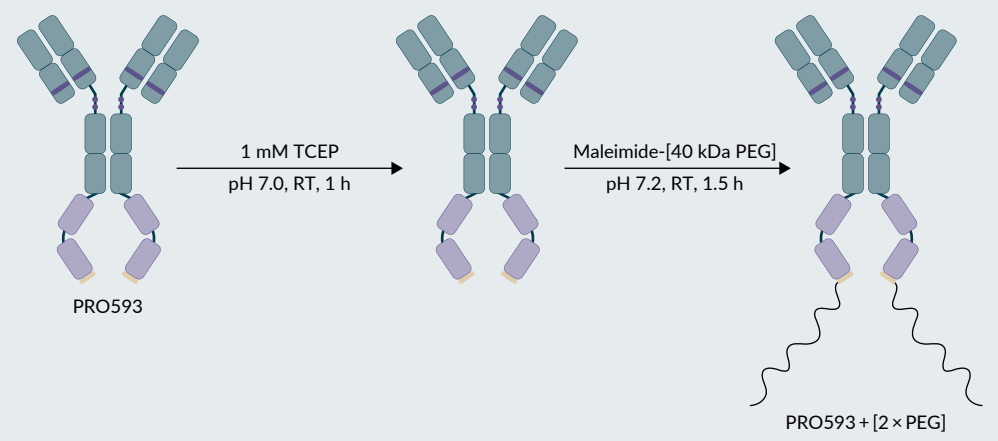

an FPLC system, and the resulting fractions were assessed for purity by SDS-PAGE. PRO593 + [2 × 40 kDa PEG] was found to elute early in the gradient, followed by unmodified PRO593. Fractions corresponding to doubly PEG-modified PRO593 were pooled and analyzed by SDS-PAGE, SEC-HPLC, and binding by SPR, as shown in **Figure 9**.

Non-reduced SDS-PAGE analysis revealed PRO504 migrates as a single band at the expected molecular weight and purity of >90% by densitometry, whereas PRO593 + [2 × 40 kDa PEG] migrates as four bands. PRO593 lacks four disulfide bonds compared to PRO504, which likely allows for dissociation under the denaturing conditions of the gel electrophoresis. From slowest to fastest migration, the bands are assigned as high molecular weight species (~8%), the PEG conjugated heavy chain dimer (~55%), the PEG conjugated heavy chain monomer (~6%), and the unpaired light chain (~31%).

Analysis by SEC-HPLC measured at >90% main peak, indicating that the dissociation observed in the electrophoresis does not occur under non-denaturing conditions. PRO504 and PRO593 + [2 × 40 kDa PEG] had retention times of 13.5 min and 11.1 min. The comparison of retention times between unmodified and PEG-conjugated material indicates that PRO593 + [2 × 40 kDa PEG] has a larger hydrodynamic radius than PRO504, as expected.

Unmodified PRO504 and PRO593 + [2 × 40 kDa PEG] bound the extracellular domain of the target receptor, protein A, and the soluble-signaling protein B, with comparable equilibrium binding constants **(Figure 9C)**.

After confirming binding and purity, the test articles were formulated, tested for endotoxin, and used in an ocular pharmacokinetics study.

PRO504 Ocular PK Study

The half-lives of PRO504 and PRO593 + [2 × 40 kDa PEG] in the vitreous of New Zealand rabbits were 4.8 and 8 days, respectively **(Figure 10A and B).** As expected, the PEG-conjugated construct was retained longer in the vitreous due to its larger hydrodynamic radius.

CONCLUSIONS

Cysteine variants were designed and evaluated for an antibody and an

FIGURE 9

Characterization of PRO504 and PRO593 + [2 × 40 kDa PEG] by (A) SDS-PAGE, (B) SEC-HPLC, and (C) KD to target proteins A and B by SPR.

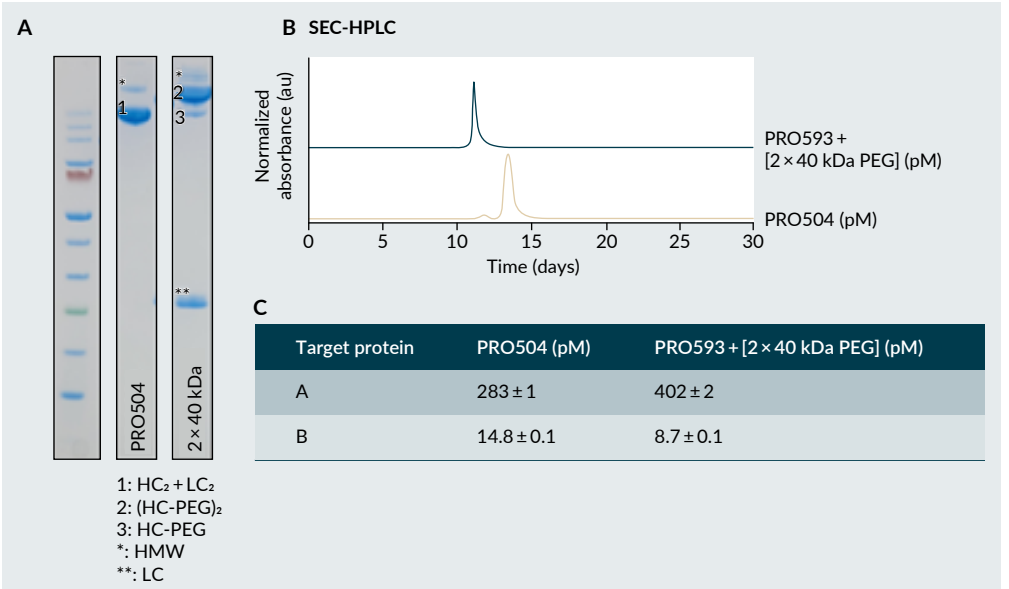

C

Target protein	PRO504 (pM)	PRO593 + [2 × 40 kDa PEG] (pM)
A	283 ± 1	402 ± 2
B	14.8 ± 0.1	8.7 ± 0.1

FIGURE 10

Total drug measured in vitreous humor by ELISA for (A) PRO504, and (B) PRO593 + [2 × 40 kDa PEG].

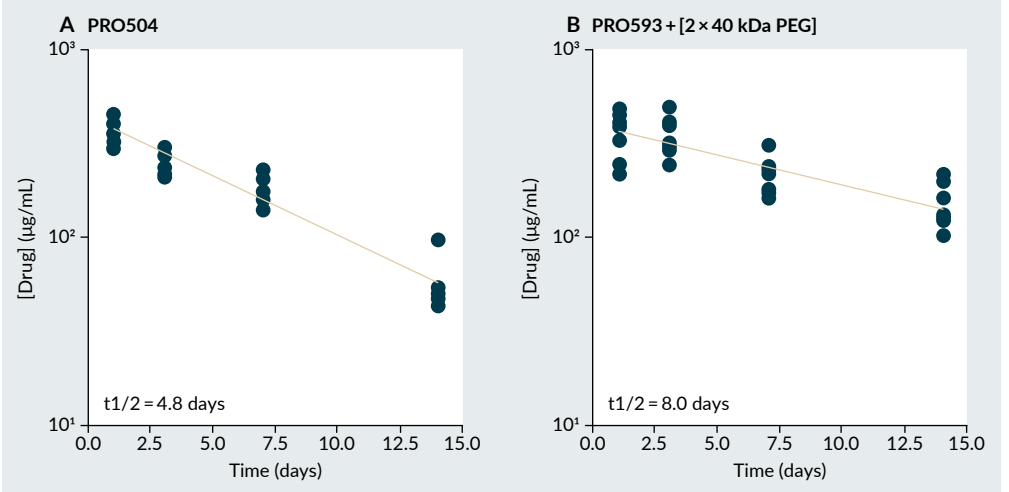

antibody-receptor domain fusion protein, PRO085 and PRO504, to enable the attachment of a maleimide-functionalized PEG and extend the ocular retention of each protein. After an initial screen of 14 variants for PRO085, PRO171 was selected for scale-up due to its efficient conversion to the desired doubly PEG-conjugated antibody. PRO171 + [2 × 5 kDa PEG] and PRO171 + [2 × 20 kDa PEG] were >90% pure and bound the target antigen comparably to the parental antibody, PRO085. In an ocular pharmacokinetic study, PRO171 + [2 × 20 kDa PEG] had the

most extended vitreous half-life of 4.8 days, followed by PRO171 + [2 × 5 kDa PEG] at 3.5 days, and finally unmodified PRO085 at 2.9 days. The half-life of PRO17 + [2 × 20 kDa PEG] was also superior to the approved intravitreal drug aflibercept.

Applying the insights from PRO085 conjugation efforts, 5 cysteine variants were produced for PRO504, and PRO593 was selected for scale-up due to its near quantitative conversion to the desired doubly PEG conjugated product. PRO593 + [2 × 40 kDa PEG] was >90% main peak and bound the two target proteins comparably to the parental PRO504. In an ocular pharmacokinetic study, PRO593 + [2 × 40 kDa PEG] was retained longer in the vitreous than the parental PRO504, with a measured half-life of 8.0 days and 4.8 days, respectively. The slower vitreal clearance observed with the PEG-conjugated products may allow for less frequent dosing, which could enhance patient adherence and lead to improved treatment outcomes.

REFERENCES

1. Ferreira A, Sagkriotis A, Olson M, Lu J, Makin C, Milnes F. Treatment frequency and dosing interval of ranibizumab and aflibercept for neovascular age-related macular degeneration in routine clinical practice in the USA. *PLoS ONE* 2015; 10, e0133968.
2. Ehlken C, Helms M, Böhringer D, Agostini HT, Stahl A. Association of treatment adherence with real-life VA outcomes in AMD, DME, and BRVO patients. *Clin. Ophthalmol.* 2018; 12, 13–20.
3. Shatz W, Hass PE, Mathieu M, *et al.* Contribution of antibody hydrodynamic size to vitreal clearance revealed through rabbit studies using a species-matched fab. *Mol. Pharm.* 2016; 13, 2996–3003.
4. Shatz W, Hass PE, Peer N, *et al.* Identification and characterization of an octameric PEG-protein conjugate system for intravitreal long-acting delivery to the back of the eye. *PLoS ONE* 2018; 14, e0218613.
5. Sharma A, Kumar N, Kuppermann BD, Bandello F. Abicipar pegol: the non-monoclonal antibody anti-VEGF. *Eye* 2020; 34, 797–801.
6. Vollmar BS, Fei M, Liang WC, *et al.* PEGylation of anti-MerTK antibody modulates ocular biodistribution. *Bioconjug. Chem.* 2022; 33, 1837–1851.
7. Famili A, Crowell SR, Loyet KM, *et al.* Hyaluronic acid-antibody fragment bioconjugates for extended ocular pharmacokinetics. *Bioconjug. Chem.* 2019; 30, 2782–2789.
8. Chandrasekaran PR, Madanagopalan VG. KSI-301: antibody biopolymer conjugate in retinal disorders. *Ther. Adv. Ophthalmol.* 2021; 13.
9. Fisusi F, Brandy N, Wu J, Akala EO. Studies on polyethylene glycol-monoclonal antibody conjugates for fabrication of nanoparticles for biomedical applications. *J. Nanosci. Nanomed.* 2020; 4, 1–9.
10. Rodwell J, McKearn T. Linker technology: antibody-mediated delivery systems. *Nat. Biotechnol.* 1985; 3, 889–894.
11. Jao SC, Ospina SME, Berdis AJ, Starke DW, Post CB, Mieyal JJ. Computational and mutational analysis of human glutaredoxin (thioltransferase): probing the molecular basis of the low pKa of cysteine 22 and its role in catalysis. *Biochemistry* 2006; 45, 4785–4796.
12. Junutula JR, Raab H, Clark S, *et al.* Site-specific conjugation of a cytotoxic drug to an antibody improves the therapeutic index. *Nat. Biotechnol.* 2008; 26, 925–932.
13. Kang JC, Sun W, Khare P, *et al.* Engineering a HER2-specific antibody–drug conjugate to increase lysosomal delivery and therapeutic efficacy. *Nat. Biotechnol.* 2019; 37, 523–526.
14. Park SJ, Choi Y, Na YM, *et al.* Intraocular pharmacokinetics of intravitreal aflibercept (Eylea) in a rabbit model. *Invest. Ophthalmol. Vis. Sci.* 2016; 57(6), 2612–2617.

AFFILIATIONS

Stacy L Capehart, Joshua D Slocum, Tobin E Brown, Alexander D Jackson, Samantha R Summers, Peter CS Woodham, Alexei Kazantsev, Marion Weir, and **Eric S Furfine,** Mosaic Biosciences, Boulder, CO, USA

Sangyuel Han, INGENIA Therapeutics, Cambridge, MA, USA

AUTHORSHIP & CONFLICT OF INTEREST

Contributions: The named authors take responsibility for the integrity of the work as a whole, and have given their approval for this version to be published.

Acknowledgements: None.

Disclosure and potential conflicts of interest: The authors are all current or former employees, and stock holders of Mosaic Biosciences.

Funding declaration: The authors received no financial support for the research, authorship and/or publication of this article.

ARTICLE & COPYRIGHT INFORMATION

Article source: Invited; externally peer reviewed.

Submitted for peer review: Aug 29, 2025.

Revised manuscript received: Oct 28, 2025.

Publication date: Nov 12, 2025.

BIOCONJUGATION INSIGHTS

DRIVING IMPROVEMENTS IN DELIVERY AND STABILITY

SPOTLIGHT

Designing with purpose: a journey through bioconjugation and nanoparticle formulation science

INTERVIEW

"At its best, formulation science is about translating complex molecules into accessible, manufacturable, and life-changing medicines."

Lauren Coyle (*Editor, Bioconjugation Insights*) speaks to **Kondareddy Cherukula** (Investigator III, Inimmune) about innovations at the intersection of chemistry, biology, and manufacturing. It discusses challenges in vaccine and nanoparticle development, process resilience and scalability strategies, and future approaches that accelerate translational impact and therapeutic accessibility of bioconjugates.

Bioconjugation Insights 2025; 1(4), 131–135 · DOI: 10.18609/bci.2025.024

Q Can you tell us a bit about what led you into the bioconjugation field and what you are currently working on?

KC I was drawn into bioconjugation as it sits right at the intersection of chemistry and biology, where a small, intentional chemical change can have a

significant biological effect. Early in my PhD, I was fascinated by targeted nanocarriers, liposomes, and polymers that could respond to disease microenvironments, and I realized how elegantly a conjugate could alter a molecule's behavior, whether it is improving half-life, directing biodistribution, or fine-tuning immune recognition.

That curiosity evolved into a passion for designing molecular bridges with purpose. Over the years, I have worked across protein–hapten, peptide, aptamers, and large-molecule conjugates, and more recently, integrated them into nanoparticle and vaccine systems. What keeps me excited is the creativity, balancing chemistry, biology, and manufacturability in one ecosystem.

Right now, a significant part of my work involves translational vaccine development, particularly tackling the opioid crisis. Our group, together with collaborators at Boston Children's Hospital, is advancing anti-fentanyl conjugate vaccines supported by the NIH HEAL Initiative. These vaccines pair a fentanyl hapten conjugated to a carrier protein with a novel adjuvant system to elicit strong neutralizing antibodies that block opioid entry into the brain. The most rewarding part is seeing science align with societal need; it is not just about elegant chemistry but potentially preventing overdose deaths. That blend of impact and innovation is exactly why I love this field.

Q What are the most critical formulation challenges in maintaining structural and functional integrity during process development and scale-up in bioconjugation vaccine platforms and nanoparticle-based therapeutics?

KC One of the biggest challenges is that conjugates are living systems; their chemistry, structure, and function are tightly intertwined. What appears homogeneous at a small scale can behave entirely differently under process stress. Mixing shear, hold time, or filtration pressure changes can subtly shift aggregation or conjugation ratios.

To manage that, I rely on a QbD approach, mapping critical process parameters (CPPs) such as conjugation stoichiometry, pH, and temperature to critical quality attributes (CQAs) such as antigenicity or aggregation state. I use orthogonal analytical tools, DLS, SDS-PAGE, and MALDI-TOF to monitor those attributes in real time and detect deviations before they affect potency. When scaling up, I prefer small-scale 'engineering mimics' that reproduce real GMP stresses, so there are no late surprises.

Maintaining hapten density, carrier integrity, and adjuvant compatibility simultaneously is no small feat, especially in conjugate vaccines. The goal is not just reproducibility, it is resilience. Designing a process that behaves predictably, regardless of scale, is the accurate measure of good formulation science.

> "The goal is not just reproducibility, it is resilience. Designing a process that behaves predictably, regardless of scale, is the accurate measure of good formulation science."

Q Nanoparticle-based therapeutics present unique stability profiling challenges compared to traditional formulations. Can you describe your approach to stability assessments and what failure mechanisms you monitor most closely in these complex systems?

KC Nanoparticles are fascinating as they are dynamic; they evolve. Thus, I approach stability from colloidal, chemical, and functional angles. I have learned that the earliest signs of instability often precede functional failure. Tracking those subtle changes is as essential as endpoint assays. When dealing with immune-active nanoparticles or conjugate–adjuvant combinations, mechanistic stress mapping, examining how temperature, freeze–thaw cycles, or mechanical agitation affect colloidal behavior, is also integrated. In short, stability work is about being proactive, not reactive, using analytics as an early warning system rather than a post-mortem.

Q How do you balance formulation stability requirements with manufacturability and scalability when working with CDMOs and preparing for GMP manufacturing? What trade-offs have you found most challenging to navigate?

KC That balance is part science, part diplomacy. Every formulation scientist has a 'perfect lab recipe' that falls apart when transferred to the GMP system. I focus on aligning early with CDMO capabilities, understanding their mixing technologies, scale-up capacity, and environmental constraints, and then reverse-engineering robustness into the formulation.

My process begins with a Target Product and Process Profile (TPP) that clearly defines what is critical versus what is flexible. For example, if a buffer system provides marginal stability gains but complicates filtration or protein stability, the system is simplified. It is more beneficial to have a formulation that is 5% less elegant but 200% more reproducible. I also advocate for in-person tech transfer whenever possible, standing next to the operators, seeing how the process behaves at scale. It builds mutual understanding and prevents months of iterative troubleshooting. Ultimately, the best formulation does not win in the lab but performs the same way everywhere it is made.

Q What platform innovations or formulation strategies are you most excited about for enhancing stability and manufacturability across multiple development pipelines in bioconjugate and nanoparticle therapeutics?

KC The field is entering an exciting phase in bioconjugation and formulation science. On the chemistry side, site-selective and bioorthogonal conjugation technologies are revolutionizing heterogeneity control and streamlining purification. That is a significant leap forward for consistency and scalability.

In formulation, I am excited by modular excipient systems, reusable, well-characterized "backbone" formulations that can be adapted across multiple conjugate or nanoparticle platforms. It is an approach that blends innovation with regulatory efficiency, letting teams move faster without reinventing the wheel. Looking ahead, these innovations will make development more predictable and significantly shorten the path from concept to clinic, which is what patients ultimately need.

Q Lastly, where do you see the field of formulation science for bioconjugate and nanoparticle-based therapeutics going in the next few years?

KC We are moving from empirical formulation toward predictive, platform-driven formulation science. The future will rely more on data-rich experimentation, computational modeling, and AI-assisted DoE to anticipate issues before they appear.

Regulatory and funding agencies such as NIH also reward this evolution, valuing deep process understanding and analytical transparency over trial-and-error optimization. Companies that can show why their formulation works, not just that it works, will move faster and face fewer surprises. There is also a strong emphasis on platform readiness, reusable conjugation, and formulation architectures that can serve multiple therapeutic areas. At its best, formulation science is about translating complex molecules into accessible, manufacturable, and life-changing medicines. The next decade will be about doing that faster, smarter, and more sustainably.

BIOGRAPHY

Kondareddy Cherukula is an Investigator at Inimmune Corporation, leading innovation in next-generation vaccine and drug delivery technologies. With over 12 years of international research experience across South Korea, France, and the United States, he bridges nanotechnology, immunology, and pharmaceutical engineering to transform molecular ideas into clinical solutions. A recipient of France's prestigious Fondation ARC Young Investigator Grant and the Young Investigator Award (2018), he has authored over 20 publications and contributed to multiple NIH-funded programs. His pioneering work on bioconjugate vaccines and lipid nanoparticle systems is advancing the frontier of precision immunotherapy and global vaccine innovation.

Kondareddy Cherukula, investigator at Inimmune Corporation, Missoula, Montana.

AUTHORSHIP & CONFLICT OF INTEREST

Contributions: The named author takes responsibility for the integrity of the work as a whole, and has given his approval for this version to be published.

Acknowledgements: None.

Disclosure and potential conflicts of interest: The author has received meeting support from the NIH/NIAID and holds stock in INIMMUNE.

Funding declaration: The author has received funding from the NIH.

ARTICLE & COPYRIGHT INFORMATION

Article source: Invited.

Interview conducted: Oct 8, 2025.

Revised manuscript received: Oct 14, 2025.

Publication date: Oct 28, 2025.

BIOCONJUGATION INSIGHTS

DRIVING IMPROVEMENTS IN DELIVERY AND STABILITY

SPOTLIGHT

Industry insights, October 2025

Lauren Coyle

Bioconjugation Insights is delighted to bring you all the latest news in the bioconjugation space in this new Industry Insights article. Brought to you by the Launch Commissioning Editor, Lauren Coyle, this article highlights the latest collaborations, regulatory changes, marketing trends, and R&D in the field. Additionally, it provides insights into key clinical trials, innovations in tools and technology, and notable conferences and publications.

Bioconjugation Insights 2025; 1(4), 157–163 · DOI: 10.18609/bci.2025.027

COLLABORATIONS AND PARTNERSHIPS

Boehringer Ingelheim bets $991M on Korean ADC program [1]

Boehringer Ingelheim has struck a deal worth up to $991M to license one of AimedBio's ADCs for development across multiple cancers. The ADC combines a tumor-targeting antibody with an exatecan-based payload and is expected to enter first-in-human trials in 2026. AimedBio will receive an upfront payment plus milestone and royalty potential. The agreement expands Boehringer's growing ADC portfolio, built on its 2020 NBE-Therapeutics acquisition and a $1.3B Synaffix deal earlier this year. The company also recently opened a new ADC R&D facility in Basel to accelerate next-generation oncology programs.

Tempus and Whitehawk Therapeutics collaborate to accelerate AI-driven ADC development [2]

Tempus AI has formed a multi-year partnership with Whitehawk Therapeutics to apply AI and real-world multimodal data to advance the development of ADCs. Using Tempus' de-identified clinical and molecular dataset, Whitehawk will optimize trial design and biomarker strategy across its ADC portfolio, which includes assets targeting PTK7, MUC16, and SEZ6 in lung and gynecological cancers. The collaboration aims to refine patient selection and indication prioritization through RNA- and IHC-based biomarker concordance,

ultimately accelerating the delivery of data-driven, targeted ADC therapies to patients with high unmet needs.

Catalent licenses Lista's certepeptide for next-generation ADC development [3]

Catalent has entered a global, non-exclusive licensing agreement with Lisata Therapeutics to integrate Lisata's certepetide, a proprietary internalizing RGD ('iRGD') cyclic peptide, into ADCs developed on Catalent's SMARTag® platform. The deal grants Catalent worldwide rights to develop and commercialize ADCs containing certepetide and its analogs, with the option to partner externally. Lisata will receive over $10M in milestone payments plus revenue sharing on future products. The collaboration aims to harness iRGD's tumor-targeting and penetration abilities to enhance ADC efficacy, with supporting preclinical data set to be presented at the World ADC conference in San Diego

Turbine and AstraZeneca partner to accelerate ADC discovery with AI-driven virtual biology [4]

Turbine has announced a new collaboration with AstraZeneca to apply its AI-powered Virtual Lab platform to ADC discovery and optimization. The partnership will leverage Turbine's simulation technology to predict ADC response mechanisms, guide sad and target selection, and reduce reliance on large-scale cell line and PDX screening. Using AstraZeneca's ADC datasets, Turbine's lab-in-the-loop approach will identify key cell lines for validation while modeling thousands of virtual experiments to predict efficacy and resistance patterns. The collaboration aims to streamline ADC development, uncover mechanistic insights, and enhance translational potential from discovery through clinical application.

REGULATORY CHANGES AND UPDATES

Mabwell's CDH17-targeting ADC 7MW4911 receives dual IND clearance in China and US5 [5]

Mabwell has secured IND clearance from China's NMPA and the US FDA for 7MW4911, a first-in-class CDH17-targeting ADC for advanced gastrointestinal cancers. Developed via

Mabwell's proprietary IDDC™ platform, 7MW4911 combines the CDH17-specific antibody Mab0727, a novel cleavable linker, and the MF-6 DNA topoisomerase I inhibitor payload. Preclinical studies showed potent antitumor activity, including efficacy in multidrug-resistant and low-CDH17-expressing models, with strong safety and pharmacokinetic profiles. The ADC's broad activity across colorectal, gastric, and pancreatic cancers underscores its potential as a next-generation bioconjugate therapy for solid tumors.

Thousand Oaks Biologics earns EU QP Declaration for ADC manufacturing facility [6]

WuXi XDC Cayman, a leading global CRDMO for bioconjugates, reports 62.2% year-on-year revenue growth to RMB 2.7 billion in 1H 2025, with gross profit up 82.2% to RMB 975 million and adjusted net profit before interest up to 69.9% to RMB 733 million. The company expanded its global customer base to 563, signed 37 new iCMC projects, and grew its backlog to $1.3 billion. Key milestones included the GMP release of the DP3 facility in Wuxi and mechanical completion of its Singapore site, on track for GMP release in 1H 2026. WuXi XDC continues advancing frontier technologies to strengthen global leadership in ADCs and bioconjugates.

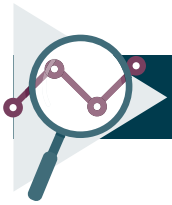

MARKET TRENDS

ADC Therapeutics raises $60M in private placement [7]

ADC Therapeutics has entered a $60M private investment in public equity (PIPE) financing, selling 11.3M common shares at $4 each and pre-funded warrants for 3.8M shares at $3.90. The round, led by TCGX with participation from Redmile Group and other investors, is expected to close on October 27, 2025. Proceeds will fund the commercial expansion and planned 2027 relaunch of its flagship ADC therapy ZYNLONTA®, strengthen the balance sheet, and support general operations. CEO Ameet Mallik said the financing positions the company for long-term growth, with key data catalysts expected through 2026.

CLINICAL TRIALS AND RESEARCH

Daiichi Sankyo's first-in-human DS-3939 ADC shows early efficacy in advanced solid tumors [8]

Initial Phase I/II results for Daiichi Sankyo's DS-3939—a potential first-in-class ADC targeting tumor-associated mucin-1 (TA-MUC1)—demonstrated encouraging antitumor activity and a manageable safety profile in heavily pretreated patients with advanced solid tumors. Presented at the ESMO Congress 2025, the dose-escalation data from

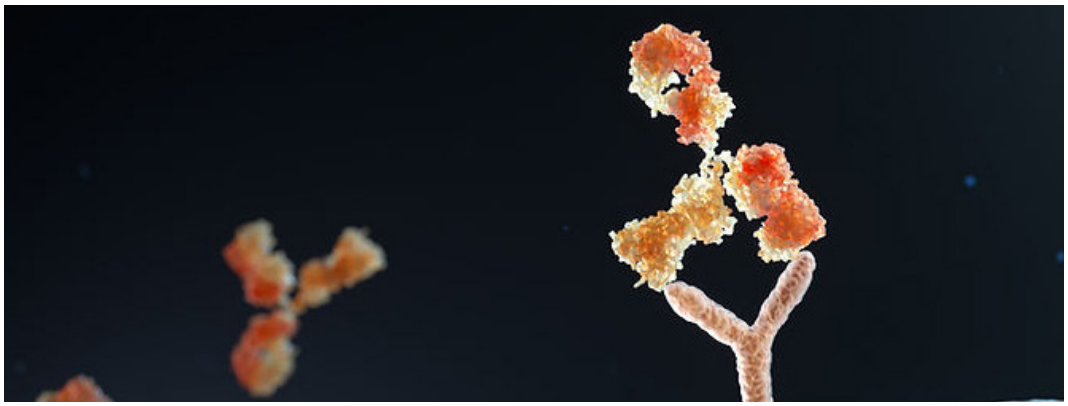

64 participants showed one confirmed complete response and 10 partial responses across ovarian, NSCLC, and breast cancers, plus 39 cases of stable disease. DS-3939 employs Daiichi Sankyo's DXd platform, linking a humanized anti-TA-MUC1 antibody to a topoisomerase I inhibitor payload. Enrollment continues globally in dose-expansion cohorts to further define its therapeutic potential.

Adcytherix secures $122M for clinical advances [9]

French ADC biotech, Adcytherix, has raised $122M in a Series A to advamce its lead ADC, ADCX-020, into clinical trials. The round, led by Bpifrance and existing investors, triples its June 2024 seed funding. Adcytherix plans US, UK, Canadian, and European trial filings by year-end while expanding its ADC pipeline. CEO Jack Elands called the financing a validation of the company's science and rapid progress since its founding 18 months ago.

Tubulis raises $361M to advance ADC pipeline and expand clinical research [10]

Tubulis has raised $361M in a Series C round led by Venrock Healthcare Capital Partners, joined by Wellington Management and Ascenta Capital. The funds will accelerate development of lead ADC TUB-040, targeting NaPi2b in ovarian and lung cancers, which holds FDA Fast Track status and is in Phase I/IIa trials. Proceeds will also support TUB-030, preclinical ADCs, and platform expansion. CEO Dr. Dominik Schumacher said the financing underscores confidence in Tubulis' vision to deliver differentiated ADCs that offer superior therapeutic benefits.

TOOLS AND TECHNOLOGIES

MEDSIR and Ataraxis AI launch AI platform to optimize ADC use in breast cancer [11]

Spanish oncology group MEDSIR has teamed up with New York-based Ataraxis AI to integrate an AI platform into breast cancer trials, aiming to improve the prediction of

patient responses and personalize treatment selection. MEDSIR will employ Ataraxis' AI-powered Breast platform, which merges pathology and clinical data to forecast outcomes for therapies including ADCs. The collaboration seeks to refine drug-matching strategies in an increasingly complex therapeutic landscape, advancing precision oncology and optimizing the clinical application of ADCs in breast cancer management.

CONFERENCE, EVENTS, AND PUBLICATIONS

SystImmune and Bristol Myers Squibb present first global data for bispecific ADC iza-bren at ESMO 2025 [12]

SystImmune and Bristol Myers Squibb unveiled the first global Phase I data for iza-bren (BL-B01D1), a first-in-class EGFR×HER3 bispecific ADC, at the ESMO Congress 2025. In the US-Lung-101 trial (NCT05983432), iza-bren showed a 55% confirmed response rate at the 2.5 mg/kg dose and a median progression-free survival of 5.4 months in heavily pretreated patients with advanced NSCLC, both EGFR-mutant and wild-type. The ADC demonstrated a manageable safety profile with primarily hematologic adverse events and no interstitial lung disease. Granted FDA Breakthrough Therapy Designation, iza-bren is now advancing into global registrational studies across lung, breast, and urothelial cancers.

Corbus to present updated Phase I/II data on next-generation Nectin-4 ADC at ESMO 2025 [13]

Corbus Pharmaceuticals will present new data at the ESMO Congress 2025 from its ongoing Phase I/II trial of CRB-701 (SYS6002), a next-generation Nectin-4-targeting ADC for advanced solid tumors. Based on a September 2025 data cut, the updated results include efficacy findings from 122 evaluable patients across head and neck, cervical, urothelial, and other cancers. CRB-701 features a site-specific, cleavable linker and a homogenous DAR of 2 with an MMAE payload. Granted FDA Fast Track status, CRB-701 is designed to improve precision and tolerability over earlier Nectin-4 ADCs.

Cellectar presents preclinical data for novel actinium-based radioconjugate in pancreatic cancer [14]

Cellectar Biosciences unveiled promising preclinical results for CLR 225, its investigational actinium-225 radioconjugate targeting pancreatic ductal adenocarcinoma (PDAC), at the AACR Special Conference on Pancreatic Cancer. CLR 225 demonstrated potent anti-tumor activity, selective biodistribution, and strong uptake across multiple pancreatic cancer xenograft models. The agent showed meaningful tumor inhibition, survival benefit, and favorable safety with no observed toxicities. Having completed IND-enabling studies, CLR 225 is positioned to advance into Phase I trials, representing a novel bioconjugate approach to overcoming the delivery barriers of dense pancreatic tumors and improving therapeutic outcomes.

Iksuda to unveil Phase I data for HER2-targeting ADC at ESMO 2025 [15]

Iksuda Therapeutics will present new clinical data on IKS014, its HER2-targeting ADC, at the ESMO Congress 2025 in Berlin. The Phase I, open-label, multicenter study (NCT05872295) assesses IKS014 in patients with advanced or metastatic HER2-positive solid tumors. Results from the dose-escalation phase conducted in Australia will highlight safety, tolerability, pharmacokinetics, pharmacodynamics, immunogenicity, and preliminary efficacy, supporting dose selection for Phase 2 development. IKS014 represents Iksuda's lead clinical ADC, developed to enhance tumor specificity and therapeutic potency across HER2-expressing cancers.

Tubulis reports positive first-in-human data for NaPi2b-targeting ADC TUB-040 at ESMO 2025 [16]

Tubulis unveiled encouraging early clinical results from its NAPISTAR1-01 Phase I/IIa study (NCT06303505) of TUB-040, a NaPi2b-targeting ADC, in platinum-resistant high-grade serous ovarian cancer (PROC-HGSOC) at the ESMO Congress 2025. Among patients treated at 1.67–3.3 mg/kg, TUB-040 achieved an objective response rate of 59% and a disease control rate of 96%, including responses in those previously treated with other ADCs. The therapy was well tolerated, with mostly low-grade hematologic adverse events and no ocular, neuropathic, or pulmonary toxicity. The data validate Tubulis' Tubutecan platform and establish proof of concept for its differentiated ADC design, supporting plans for pivotal trials and expansion into new tumor types.

SUMMARY

The bioconjugation sector continues its rapid expansion with major collaborations, regulatory milestones, and significant clinical and financing activity. Boehringer Ingelheim strengthened its oncology portfolio through a $991M licensing deal with Korea's AimedBio, while Tempus AI and Whitehawk Therapeutics formed a data-driven alliance to advance biomarker-based ADC development. Catalent partnered with Lisata Therapeutics to integrate certepetide into its SMARTag platform, and AstraZeneca teamed up with Turbine to leverage AI-powered cell simulations for ADC discovery.

On the regulatory front, Mabwell secured dual IND clearance in China and the US for its CDH17-targeting ADC 7MW4911, and Thousand Oaks Biologics' Shanghai facility earned EU QP certification, confirming GMP compliance for ADC manufacturing. Financing momentum remained strong: ADC Therapeutics raised $60M to support the relaunch of ZYNLONTA, while European firms Adcytherix and Tubulis closed $122M and $361M rounds, respectively, to accelerate clinical and pipeline development.

At the ESMO Congress 2025, several companies presented promising ADC data. Daiichi Sankyo's DS-3939 showed durable responses in multiple solid tumors; SystImmune and Bristol Myers Squibb reported a 55% response rate for their bispecific EGFR×HER3 ADC iza-bren; Corbus Pharmaceuticals showcased progress with

its next-generation Nectin-4 ADC; Iksuda unveiled first-in-human data for IKS014; and Tubulis' NaPi2b-targeting TUB-040 achieved a 59% response rate in ovarian cancer. Together, these results underscore the field's accelerating clinical maturity and innovation across platforms, targets, and modalities.

REFERENCES

1. Boehringer Ingelheim. Oct 15, 2025. https://www.boehringer-ingelheim.com/science-innovation/human-health-innovation/new-partnership-helps-advance-our-cancer-adcs-portfolio.
2. Tempus. Oct 16, 2025. https://www.tempus.com/news/pr/tempus-announces-collaboration-with-whitehawk-therapeutics-to-advance-biomarker-driven-oncology-research/?utm_source=linkedin&utm_medium=organic_social&utm_campaign=whitehawk_collab&utm_term=october_2025&utm_content=learn_more&srsltid=AfmBOorDT4dn0i3rO9ZxZjr54-yPGnp-0jsAeYJ9pMSwGSJH4v0A90Zp.
3. Lisata Therapeutics. Oct 8, 2025. https://ir.lisata.com/news-releases/news-release-details/lisata-therapeutics-and-catalent-announce-global-antibody-drug.
4. Turbine AI. Oct 9, 2025. https://turbine.ai/announcements/turbine-launches-collaboration-with-astrazeneca-leveraging-turbines-virtual-disease-models-to-rationalize-adc-discovery.
5. Mabwell. Oct 13, 2025. https://www.mabwell.com/en/news_info/id-194.html.
6. Thousand Oaks Biologics. Oct 11, 2025. https://www.tobiopharm.com/news/70.
7. ADC Therapeutics. Oct 13, 2025. https://ir.adctherapeutics.com/press-releases/press-release-details/2025/ADC-Therapeutics-Announces-60-Million-Private-Placement/default.aspx.
8. Daiichi Sankyo. Oct 19, 2025. https://daiichisankyo.us/press-releases/-/article/ds-3939-shows-promising-preliminary-clinical-activity-in-patients-with-advanced-solid-tumors-in-phase-1-2-trial.
9. Adcytherix. Oct 16, 2025. https://www.adcytherix.com/post/adcytherix-raises-eur-105m-series-a-to-accelerate-breakthrough-antibody-drug-conjugate-pipeline-with.
10. Tubulis. Oct 15, 2025. https://tubulis.com/news/tubulis-raises-e308-million-series-c-to-accelerate-clinical-development-of-lead-adc-candidate-tub-040-and-expand-pipeline.
11. MEDSIR. Oct 2, 2025. https://www.medsir.org/post/medsir-and-ataraxis-ai-launch-research-collaboration-to-evaluate-ai-powered-platform-as-a-predictive.
12. Systimmune. Oct 17, 2025. https://systimmune.com/news---systimmune-inc-and-bristol-myers-squibb-announce-first-global-phase-i-results-of-iza-bren-an-egfr-x-her3-bispecific-antibody-drug-conjugate-in-patients-with-advanced-solid-tumors-at-esmo-2025.
13. Corbus Pharmaceuticals. Oct 14, 2025. https://ir.corbuspharma.com/news-events/press-releases/detail/451/corbus-pharmaceuticals-to-present-crb-701-phase-12-data-at-esmo-2025..
14. Cellectar Biosciences. Oct 14, 2025. https://investor.cellectar.com/press-releases/detail/378/cellectar-biosciences-presented-promising-preclinical-data.
15. Iksuda. Oct 14, 2025. https://www.iksuda.com/news-views/iksuda-to-present-iks014-phase-1-data-at-esmo.
16. Tubulis. Oct 19, 2025. https://tubulis.com/news/tubulis-presents-first-clinical-data-from-phase-i-iia-trial-for-tub-040-in-platinum-resistant-ovarian-cancer-proc-at-esmo-2025.

Lauren Coyle is the Launch Commissioning Editor of *Bioconjugation Insights*

BIOCONJUGATION INSIGHTS

Challenges and future directions of dual payload antibody–drug conjugates

Rakesh Dixit

EDITORIAL

"Determining optimal dosing for dpADCs represents a multidimensional optimization problem that extends beyond traditional maximum tolerated dose identification."

Bioconjugation Insights 2025; 1(4), 137–141 · DOI: 10.18609/bci.2025.025

Dual-payload ADCs represent an emerging strategy to address tumor heterogeneity and resistance mechanisms by delivering two distinct cytotoxic agents via a single antibody scaffold. While this approach offers potential advantages in therapeutic breadth and efficacy, it introduces substantial challenges across the development spectrum. Complex linker chemistry, heterogeneous drug-to-antibody ratios, increased hydrophobicity, and complex analytical characterization complicate manufacturing and scale-up. Translational hurdles include non-overlapping pharmacokinetic profiles, toxicity attribution difficulties, and intricate clinical trial design requirements. Recent innovations in orthogonal conjugation platforms, site-specific chemistry, and model-informed development strategies are beginning to address these obstacles. With multiple dual-payload ADC programs now entering clinical evaluation, the field stands

at a critical juncture where scientific ingenuity must converge with manufacturing pragmatism to realize the therapeutic promise of dual-payload platforms.

RATIONALE FOR DUAL-PAYLOAD STRATEGIES

Single-payload ADCs have transformed oncology treatment over the past decade, but tumor heterogeneity and acquired resistance continue to limit their efficacy. Tumors frequently exhibit variable antigen expression across cell populations, and cancer cells can develop resistance through multiple mechanisms, including drug efflux pump upregulation, target antigen downregulation, and alterations in apoptotic machinery. Dual-payload ADCs (dpADCs) aim to overcome these limitations by simultaneously delivering two cytotoxic agents with complementary or synergistic mechanisms of action.

The conceptual appeal is straightforward: a topoisomerase I inhibitor combined with a microtubule inhibitor can attack cancer cells through orthogonal pathways, potentially reducing the likelihood of resistance emergence. Similarly, pairing a membrane-permeable bystander payload with a cell-resident agent addresses both antigen-positive tumor cells and neighboring heterogeneous populations that may lack target expression. However, translating this biological rationale into manufacturable, clinically viable therapeutics presents formidable technical challenges that span chemistry, manufacturing, controls, and clinical development.

SCIENTIFIC & TECHNICAL CHALLENGES OF dpADCs

Linker chemistry complexity and payload release control

Conjugating two distinct payloads to a single antibody scaffold requires orthogonal linker strategies that maintain chemical selectivity throughout synthesis while ensuring appropriate stability and release kinetics in vivo. The linker must remain stable in circulation to prevent premature payload release and systemic toxicity yet efficiently liberate both drugs within target cells following internalization and trafficking to lysosomes.

Recent advances in linker design offer multiple strategies to address these competing demands. Mix-and-match approaches combine a bystander-capable payload, such as monomethyl auristatin E (MMAE) or deruxtecan (DXd) on a cleavable linker, with a cell-resident payload like monomethyl auristatin F (MMAF) on a non-cleavable linker. This configuration balances efficacy against heterogeneous tumors while limiting systemic toxicity from membrane-permeable cytotoxins.

Tandem-cleavage linkers represent another innovation, employing glucuronide caps that require sequential enzymatic removal within lysosomes before payload release. This dual-barrier approach prevents extracellular protease cleavage and has demonstrated reduced hematologic toxicity in preclinical models. Peptide sequences can be tuned through motifs such as glutamate-valine-citrulline, valine-alanine, or other modified sequences to adjust plasma stability, cathepsin specificity, and release kinetics independently for each payload.

Click-to-release chemistry utilizing bioorthogonal pairs such as trans-cyclooctene and tetrazine enables triggered payload liberation, allowing one drug to be released lysosomally. At the same time, another can be activated externally at a defined time point. Site-specific and orthogonal conjugation methods—employing azide-DBCO and methyltetrazine-TCO click chemistry or enzymatic tagging—provide precise control over drug-to-antibody ratios (DAR) and minimize heterogeneity in dual-payload constructs.

Stabilized maleimide chemistries address the retro-Michael deconjugation problem inherent to traditional cysteine-maleimide adducts through self-hydrolyzing maleimides or post-conjugation ring-opening strategies. Alternative enzyme triggers, including β-glucuronidase or sulfatase-cleavable linkers, offer orthogonal payload release mechanisms, enabling independent control of each drug's liberation within the same ADC construct.

DAR control and product heterogeneity

Dual payloads amplify the heterogeneity challenges already present in single-payload ADC development. Rather than achieving a uniform DAR of 4 or 8, dual-payload systems must control both total DAR and the relative ratio between payload A and payload B. A nominally '4+2' construct may exist as a distribution of species: 4+2, 3+3, 5+1, and other combinations, each with potentially different pharmacokinetic (PK) properties, efficacy, and toxicity profiles.

Both total DAR and the payload ratio constitute critical quality attributes that directly impact clinical performance. Programs such as KH815 (an anti-TROP2 dpADC combining a topoisomerase I inhibitor with an RNA polymerase II inhibitor) and IBI3020 (a dual-payload anti-CEACAM5 ADC) [1] have established tight specifications for DAR ranges (e.g., 5.8–6.2) and payload ratio tolerances (e.g., 4±0.2:2±0.2) to ensure batch-to-batch consistency.

Early adoption of site-specific conjugation platforms with orthogonal chemical handles provides the foundation for reproducible payload distribution. Enzyme-mediated tagging, branched linkers, or sequential click chemistry reactions enable controlled conjugation that scales reliably from development batches to commercial manufacturing. At the production scale, micro-mixing gradients and local reagent concentration variations can produce over-conjugated species, necessitating staged reagent feeds, validated mixing protocols, and in-process DAR monitoring.

Hydrophobicity and colloidal stability

Dual payloads, particularly when both are hydrophobic drugs such as MMAE and Exatecan derivatives, substantially increase ADC aggregation risk, reduce plasma half-life through accelerated clearance, and promote non-specific uptake in healthy tissues. Hydrophobicity is not equally distributed between payloads; MMAE contributes significantly more to hydrophobic character than MMAF, making the payload ratio selection consequential for formulation stability.

Hydrophilic masking strategies incorporate polyethylene glycol, polyethylene glycol oligomers, polysarcosine, or sulfamide groups into linker spacers to improve solubility and manufacturability at high DARs. Capping total DAR at levels that maintain acceptable hydrophobic interaction chromatography retention times represents another practical approach. Formulation development may require evaluation of lyophilized presentations to reduce free drug formation during storage, along with excipient screening to maintain colloidal stability.

Analytical characterization demands

Demonstrating consistency, stability, and bioactivity for two payloads adds substantial analytical complexity. Real-time DAR tracking through native hydrophobic interaction chromatography-mass spectrometry or intact mass spectrometry provides process control during manufacturing. Orthogonal assays must quantify each payload independently, track site-specific occupancy through peptide mapping and middle-up analysis, and measure free drug levels separately for each cytotoxin.

Preparative chromatography techniques, including mixed-mode or hydrophobic interaction chromatography, can polish DAR distributions by removing high-DAR or improperly conjugated species, supporting release consistency. Bioanalytical methods must distinguish intact ADC, total antibody, and each free payload in plasma and tissue samples—a requirement that substantially increases method development and validation burden compared to single-payload ADCs.

Forced degradation studies must separately track each payload's degradation pathway, as linker hydrolysis, payload deconjugation, and aggregation may occur at different rates for the two drugs. Potency assays present particular challenges, as regulatory agencies expect demonstration that both payloads contribute to biological activity through mechanistically relevant endpoints, not simply generic cell killing assays.

Manufacturing and scale-up challenges

The conjugation process for dpADCs typically employs sequential or one-pot approaches with orthogonal chemistry. Sequential conjugation provides clear separation between reaction steps but increases processing time and potential product loss. One-pot methods streamline manufacturing but require careful validation to prevent cross-reactivity between conjugation chemistries.

Process development must establish critical process parameters, including pH, reagent stoichiometry, mixing regime, temperature control, and antibody reduction state for thiol-based conjugations. At commercial scale, technology transfer from development laboratories to GMP manufacturing facilities requires demonstration that the process performs consistently across different equipment configurations and production sites.

Supply chain management becomes more complex with dual payloads, as two independent payload-linker supply chains must be maintained with appropriate regulatory traceability. Lead times, quality specifications, and contingency planning must account for both payloads, and manufacturing schedules must accommodate the possibility of payload-specific supply disruptions.

PRECLINICAL & CLINICAL ADAPTATIONS & DEVELOPMENT

Preclinical model adaptations for translational production

dpADCs require specialized preclinical approaches to predict human PKs and safety, as each payload exhibits distinct release mechanisms, distribution patterns, and toxicity profiles. Multi-analyte bioanalysis represents the foundation, with hybrid ligand-binding assay-liquid chromatography-mass spectrometry methods quantifying intact ADC, total antibody, each free payload, and key catabolites. DAR-resolved mass spectrometry tracks conjugation heterogeneity and differential clearance of high- versus low-DAR species.

Species selection and genetic models must account for antibody-specific considerations. Human FcRn transgenic mice align antibody salvage with human kinetics, while antigen knock-in models address situations where cynomolgus monkeys lack target cross-reactivity. Early screening in human and cynomolgus plasma identifies species differences in carboxylesterase or protease activity that may affect payload release.

Dual-tracer strategies employing multi-isotope radiolabeling enable mass balance studies and distinguish antibody versus payload localization through autoradiography and whole-body imaging. Tumor distribution studies using co-culture mosaic assays and conditioned-medium

transfer experiments assess payload-specific bystander killing, with outputs parameterizing mechanistic pharmacokinetic/pharmacodynamic (PK/PD) models of tumor penetration and kill radii.

Organ-specific toxicology platforms address poorly predictable toxicities that may emerge with dual-payload combinations. Human lung organoids evaluate topoisomerase I inhibitor payloads for interstitial lung disease risk, dorsal root ganglion neuron assays assess auristatin-mediated peripheral neuropathy, and corneal explant models predict ocular liabilities. These platforms enable earlier identification of toxicity risks than traditional animal studies alone.

Clinical trial design innovations

Determining optimal dosing for dpADCs represents a multidimensional optimization problem that extends beyond traditional maximum tolerated dose identification. Toxicities and efficacies may arise from either payload independently or from their combination, with potential for synergistic effects in both therapeutic and adverse domains.

Two-dimensional dose exploration treats dose-finding as a problem accounting for exposures to both payloads. Model-assisted designs, such as Bayesian optimal interval-combo methods, identify tolerable dose regions rather than single maximum tolerated doses. Parallel testing of different DAR configurations or payload ratios allows adaptive selection of the most favorable formulation during early clinical development.

Time-to-event toxicity modeling addresses late-onset adverse events characteristic of ADCs, including interstitial lung disease, ocular toxicities, and peripheral neuropathy that may emerge beyond cycle one. Time-to-event continual reassessment method or time-to-event Bayesian optimal interval designs allow dose escalation to continue while accounting for incompletely observed toxicity data, improving both safety and efficiency.

Joint efficacy-toxicity optimization through seamless Phase I/II design models both endpoints simultaneously to identify optimal biologic doses that may differ from maximum tolerated doses. This approach aligns with regulatory guidance under Project Optimus, which encourages randomized dose-ranging cohorts early in development with exposure-response analyses and patient-centric tolerability endpoints.

Model-informed drug development plays a central role in dpADC programs. Extensive PK sampling for total ADC, total antibody, and free payloads enables joint exposure-response modeling. Translational physiologically based PK and population PK models inform exposure caps per payload and guide adaptive dosing algorithms. Schedule engineering through split dosing (e.g., Day 1 and Day 8 in 21-day cycles) can reduce Cmax-driven toxicities while maintaining cumulative exposure.

Intra-patient dose titration, where individual patients undergo adaptive escalation based on their PK/PD responses, may accelerate convergence on therapeutic exposure windows when inter-patient variability is high. Safety run-ins incorporating prophylactic supportive care, such as granulocyte colony-stimulating factor or ocular protection, help determine whether these measures can expand tolerable dose ranges.

BALANCING BIOLOGICAL RATIONALE WITH PRACTICAL CONSTRAINTS

Payload selection for dpADCs requires integration of mechanistic biology with chemistry, manufacturing, and controls feasibility. Tumor heterogeneity combined with multidrug resistance or efflux pump expression favors pairing a bystander payload with a non-permeable, efflux-resistant

agent. Preclinical studies in HER2 and TROP2 tumor models have demonstrated that MMAE plus MMAF dual-payload ADCs outperform either mono-payload ADC alone or co-administered single ADCs targeting the same antigen, validating this approach.

For tumors with topoisomerase I resistance or requiring deeper DNA damage, combining a topoisomerase I inhibitor with a microtubule inhibitor provides orthogonal killing mechanisms while limiting cross-resistance. The combination of topoisomerase I inhibitors with RNA polymerase II inhibitors, as exemplified by KH815 (NCT06885645), offers transcriptional shutdown alongside DNA damage and has advanced to first-in-human evaluation.

Payload ratio optimization often proves more impactful than maximizing total DAR. In MMAE plus MMAF constructs, MMAE count primarily drives hydrophobicity; configurations biased toward 4+2 (MMAE+MMAF) frequently demonstrate better efficacy and pharmacokinetics than 2+4 splits or high-DAR MMAE alone in resistant or heterogeneous tumor models. When combining orthogonal mechanisms such as topoisomerase I inhibitors with microtubule inhibitors, assigning the more permeable or bystander-capable payload to lower per-antibody stoichiometry can preserve therapeutic index while expanding kill coverage.

Linker and release logic must prioritize compatibility and orthogonality. Microbial transglutaminase Q295 tagging combined with azide-DBCO and tetrazine-TCO click pairs enables clean 4+2 builds with no cross-reactions, with both payloads releasing after lysosomal cathepsin cleavage. Branched glutamate-valine-citrulline-para-aminobenzyloxycarbonyl linkers provide plasma stability while preserving rapid lysosomal release—particularly valuable when carrying bystander warheads.

Engineering release hierarchy ensures that more lipophilic or bystander-active payloads receive slower-cleaving triggers or lower copy numbers. In contrast, cell-resident payloads such as MMAF follow slower or faster or membrane-impermeable routes, leading to greater tumor retention. This strategic asymmetry maintains therapeutic index while addressing tumor heterogeneity.

CLINICAL VALIDATION & FUTURE DIRECTIONS

The advancement of dpADC programs into clinical evaluation validates manufacturing and analytical feasibility while providing critical insights into safety management and dose-finding strategies for mixed-mechanism constructs. KH815, combining topoisomerase I and RNA polymerase II inhibitor payloads conjugated to an anti-TROP2 antibody, has entered Phase I evaluation. IBI3020, a dual-payload anti-CEACAM5 ADC, similarly reached clinical stage, demonstrating that the technical challenges of dual-payload manufacturing can be surmounted at commercial scale.

These programs will generate essential exposure-response data for each payload and the intact ADC, informing optimal DAR split selection and recommended Phase II doses. Early clinical read-outs on tolerability, bystander effect management, and the relationship between payload ratios and therapeutic index will guide second-generation design decisions across the field.

Several pitfalls must be avoided as the field matures. Treating dual-payload ADCs as simply 'two mono-ADCs on one antibody' overlooks critical pharmacologic differences; co-dosing separate ADCs targeting the same antigen creates antigen competition, whereas a single dual-payload ADC ensures both warheads reach the same internalization event. Chasing maximum total DAR without payload ratio optimization frequently compromises pharmacokinetics and solubility, as ratio tuning consistently outperforms 'more drug' approaches. Mismatched release kinetics between payloads can drive off-target toxicity if one

payload is released systemically while the other remains intracellular, demanding deliberate trigger selection and verification through orthogonal release assays.

SUMMARY

dpADCs offer a promising approach to overcome tumor heterogeneity and resistance by delivering two distinct cytotoxic agents via a single antibody, but they present significant challenges in linker chemistry, DAR control, hydrophobicity management, analytical characterization, manufacturing scale-up, and complex clinical trial designs, with recent advances and ongoing clinical programs beginning to address these issues and guide future development strategies.

REFERENCE

1. Zhao Y, Ren P, Guan M, *et al*. Abstract 1585: KH815, a novel dual-payload TROP2-directed antibody-drug conjugate, shows potent antitumor efficacy in pre-clinical tumor model. *Cancer Res*. 2025; 85 (8_suppl_1), 1585; Taylor O. Innovent biologics makes milestone advances in cancer treatment. *Investors Hangout* Apr 29, 2025. https://investorshangout.com/innovent-biologics-makes-milestone-advances-in-cancer-treatment-274344-.

AFFILIATION

Rakesh Dixit PhD DABT, Cofounder, President and Chief Scientific Officer, Regio Biosciences; Chief Executive Officer, Bionavigen Oncology, LLC; and Chief Scientific Officer, TMAB Therapeutics, Rockville, ML, USA.

AUTHORSHIP & CONFLICT OF INTEREST

Contributions: The named author takes responsibility for the integrity of the work as a whole, and has given his approval for this version to be published.

Acknowledgements: None.

Disclosure and potential conflicts of interest: The author has no conflicts of interest.

Funding declaration: The author received no financial support for the research, authorship and/or publication of this article.

ARTICLE & COPYRIGHT INFORMATION

Article source: Invited.

Revised manuscript received: Oct 16, 2025.

Publication date: Nov 4, 2025.